



INAF - IASF BOLOGNA
ISTITUTO DI ASTROFISICA SPAZIALE
E FISICA COSMICA - BOLOGNA

**Progetto Laue
EGSE Detectors Calibration
Report**

Doc: 637/2014
Issue: 1.1
Date: 2012-12-18
Pag. I / 35

Progetto LAUE – Una lente per i raggi Gamma
EGSE Detectors Calibration Report

Internal Report INAF/IASF-Bo n. 637/2014

Natalia Auricchio, Ezio Caroli, John B. Stephen, Angelo Basili



INAF - IASF BOLOGNA
ISTITUTO DI ASTRONOMIA SPAZIALE
E FISICA COSMICA - BOLOGNA

Progetto Laue
EGSE Detectors Calibration
Report

Doc: 637/2014
Issue: 1.1
Date: 2012-12-18
Pag. II/ 35

Changes History

Document Issue	Changes



TABLE OF CONTENTS

1. Subject	1
1.1 Purpose	1
2. Applicable and reference documents	1
3. Acronyms	1
4. Introduction	1
5. Imager Specifications	1
5.1 The XRD 0822 AO description	2
5.1.1 Electronic readout.....	3
5.1.2 Software description	3
5.2 Image correction: offset, gain and pixel	3
5.3 Imager characterization and calibration	4
5.3.1 Imager Stability	4
5.3.2 Sensitivity at different collimated X-ray beam intensities	5
5.3.3 Spatial resolution	6
5.3.4 Angular resolution.....	7
6. Spectrometer Specifications	9
6.1 Electronics chain description	9
6.1.1 Amplifier and Amplifier 2.....	11
6.1.2 ADC.....	12
6.1.3 High Voltage	12
6.1.4 Status	13
6.1.5 Presets	13
6.2 Software description	13
6.3 Characterization and calibration at IASF Bologna laboratory	14
6.3.1 <i>Characterization as a function of the bias voltage and amplifier shaping time</i>	14
6.3.2 <i>Characterization as a function of the energy</i>	15
6.4 Characterization at Larix facility	19
6.4.1 <i>Characterization as a function of the bias voltage and amplifier shaping time</i>	19
6.4.2 <i>Characterization as a function of the energy</i>	20
6.4.3 <i>Comparison between DSPEC-LF and Standard Nuclear Instrumentation Systems</i>	22
6.4.4 <i>Instruments interference</i>	23
6.4.5 <i>Requirement on the energy resolution</i>	24
6.4.6 <i>Spectrometer Stability</i>	25
6.4.7 <i>Background</i>	26
7. Test under X-Ray beam at LARIX	28



INAF - IASF BOLOGNA
ISTITUTO DI ASTRONOMIA SPAZIALE
E FISICA COSMICA - BOLOGNA

**Progetto Laue
EGSE Detectors Calibration
Report**

Doc: 637/2014
Issue: 1.1
Date: 2012-12-18
Pag. IV/ 35

8. Images at a different focal length	29
9. Beam intensity as a function of the collimator window	30
10. Conclusions	31



1. Subject

1.1 Purpose

The document describes the activities and tests performed to characterize and calibrate the EGSE detectors that are integrated in the X-ray beam at the LARIX facility in Ferrara.

2. Applicable and reference documents

- [DA-01] Contratto ASI I/068/09/0 ed Allegato tecnico gestionale
- [DA-02] Proposta Tecnico-Gestionale sottomessa ad ASI
- [DA-03] Science Requirement (WP 1200, UNIFE-LAUE-RP-01-10)
- [DA-04] Specifiche dell'EGSE: Definizione/Acettazione e realizzazione Rivelatore (WP 4300, IASFBO-LAUE-RP-01-10)
- [DA-05] LAUE EGSE SOFTWARE FUNCTIONAL REQUIREMENTS FOR DETECTOR DATA PROCESSING (TAS-I)
- [DA-06] WPD, PROJECT: LAUE – UNALENTE PER RAGGI GAMMA, W.P. TITLE: EGSE, integration and test (TAS-I)
- [DA-07] Scientific requirements and detectors' specification analysis (IASFBO-LAUE-SP-01-11).

3. Acronyms

ASI	Agenzia Spaziale Italiana	MCB	Multi Channel Buffer
DIM	Detector Interface Module	SW	Software
DSPEC	Detector Interface Module	TAS-I	Thales Alenia Space -Italia
HPGe	High Purity Germanium	UNIFE	Università di Ferrara
IASFBO	Istituto di Astrofisica Spaziale e Fisica Cosmica di INAF Bologna	WP/WPD	Work Package/Work Package Description
INAF	Istituto Nazionale di Astrofisica	XIS	X-Ray Imaging Software
LARIX	Large Italian X-ray facility	XRD	X-Ray Detector

4. Introduction

The detection system to be used for positioning and gluing each crystal on the lens petal frame and for qualification of the assembled petal is composed of two detectors, an imager and a spectrometer positioned in the focal plane of the Laue petal at 20 m.

5. Imager Specifications

The imager function is to acquire the images needed to determine the Bragg angle and, therefore the average direction of the chosen lattice planes of each crystal tile. The Flat Panel X-Ray Detector from Perkin Elmer satisfies the imager requirements, reported in [DA-03, DA-04, DA-07], and its specifications are described in table 5.1.

Table 5.1. Imager specifications.

Energy range (keV)	40 keV-15 MeV
Spatial resolution (micron)	200
Active area (cm ²)	20.48x20.48
Total/Active pixel number	1024x1024/1000x1000



5.1 The XRD 0822 AO description

The Digital X- Ray Detector 0822 AO is composed of a sensor and its electronics housed in one package shown in Figure 5.1 at Larix facility after integration of the EGSE system.

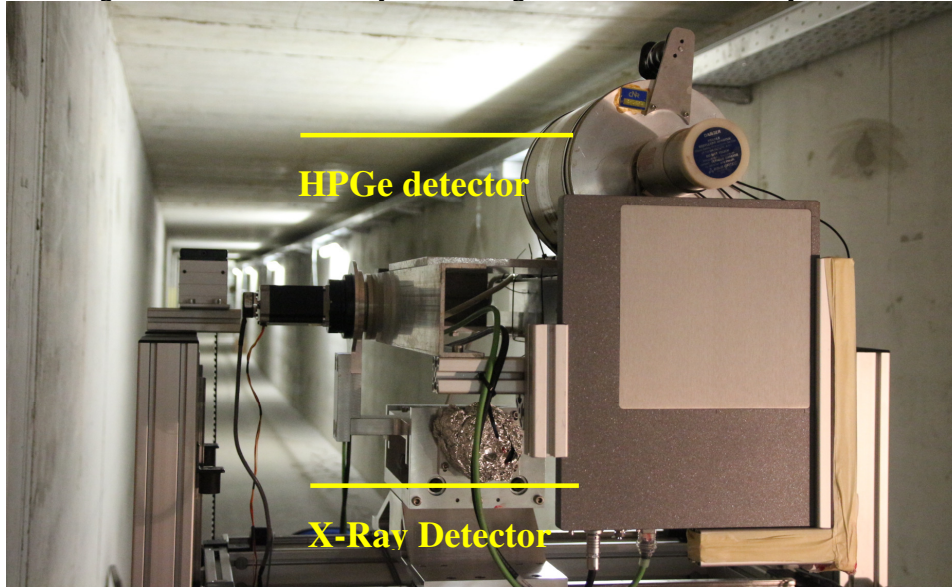


Figure 5.1. Final setup after mounting the focal plane detectors at the Larix facility. The Digital X-Ray Detector is positioned below the High Purity Germanium Detector.

The flat panel sensor of the XRD 0822 AO is fabricated using thin film technology based on amorphous silicon. Each pixel in the array consists of a light sensing photodiode and a switching thin film transistor (TFT) in the same electronic circuit. The incident X-Rays are converted by the scintillator material (CsI:TI, direct deposited on Si photodiodes) to visible light which creates electron hole pairs in the biased photodiode. The charge carriers are stored in the photodiode capacity. By turning on the gates of a TFT line within the matrix, the charges of all columns are transferred in parallel to the signal outputs. All signals of the columns are amplified in custom readout multiplexers for processing. In figure 5.2 the structure of XRD 0822 AO is displayed.

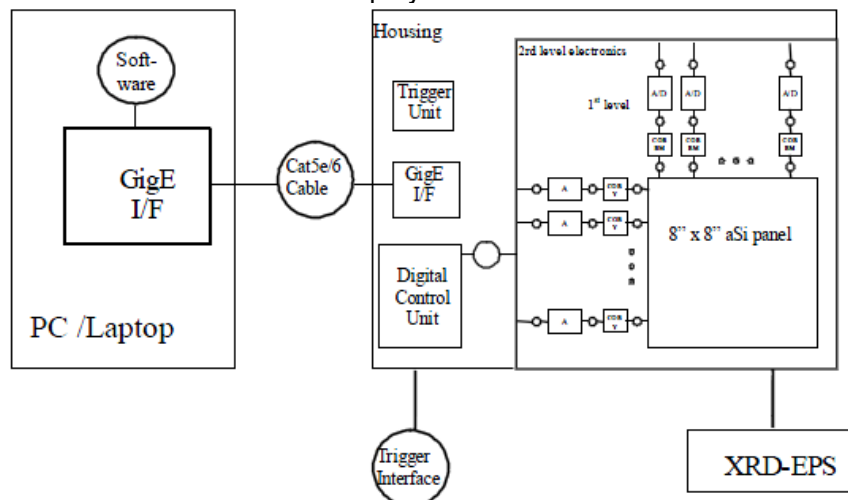


Figure 5.2. Digital X-ray Detector structure.



5.1.1 Electronic readout

Charge amplifiers for sensor readout and row drivers for addressing the rows are placed on chip on board modules contacting the pads at sensor edge. The chips on board for control and readout are connected to Analogue/Digital conversion PCB board. The analog part of the electronics is allocated beside the sensor and includes FPGA control of the detector.

In Figure 5.3 we illustrate a detail of the connections from XRD 0822 AO to PC with Gigabit Ethernet interface and from XRD-EPS power supply to the detector. This power supply is a stand-alone unit designed to support the XRD 0822 AO.

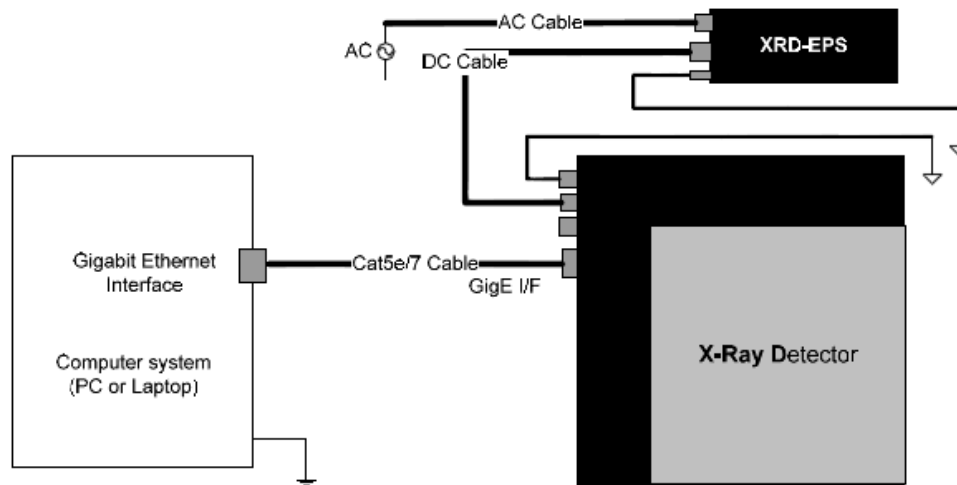


Figure 5.3. Digital X-ray Detector connections.

5.1.2 Software description

We use the commercial X-Ray Imaging Software (XIS) from Perkin Elmer to acquire and correct the images of XRD. We can set the acquisition mode, free running or triggered, the integration time from 66.6 ms to 2s, the gain, 1 or 4 pF, and the binning mode (2x2, in this case the pixel size becomes $0.4 \times 0.4 \text{ mm}^2$). Significant feature is the acquisition not only of one single image at the selected frame time but also of a sequence of n images (n depending of PC performances).

5.2 Image correction: offset, gain and pixel

Each column is connected to one channel of the readout electronics with the specific channel offset resulting in a dark image with vertical stripes caused by the individual channel offset. The dark image may also contain pixels which are brighter than the others caused by a higher dark current.

The detector is arranged in groups of 128 readout channels. The groups can deviate in gain and it is possible to distinguish blocks of 128 channels in an image due to this gain difference. The sensor itself may have pixels and rows or columns underperforming, e.g. defective because totally black or white.

As a consequence the XRD needs an offset correction to take into account the dark current of each pixel. During the warm-up phase of the detector, the offset is not stable and during this period the detector use is not recommended. During operating activity it is important to refresh periodically the offset.

To homogenize the differences in pixel sensitivity we can also perform a gain correction, in which the whole image area has to be illuminated homogeneously in an optimum dynamic range of the sensor (70/80 % of the full scale range).



The Pixel correction allows a “software repair” of underperforming pixels to enhance image quality. Underperforming pixel values are replaced with the averaged value of the surrounding eight adjacent pixels. The pixel correction is only performed on specific pixels, mapped in the file PXLMASK.his, included in the package together the offset and gain correction at 66.6 ms.

In the following figure we report the delivered pixel and gain correction images, while in successive figure an acquired image before and after correction using our files produced at the same experimental conditions at Larix facility:

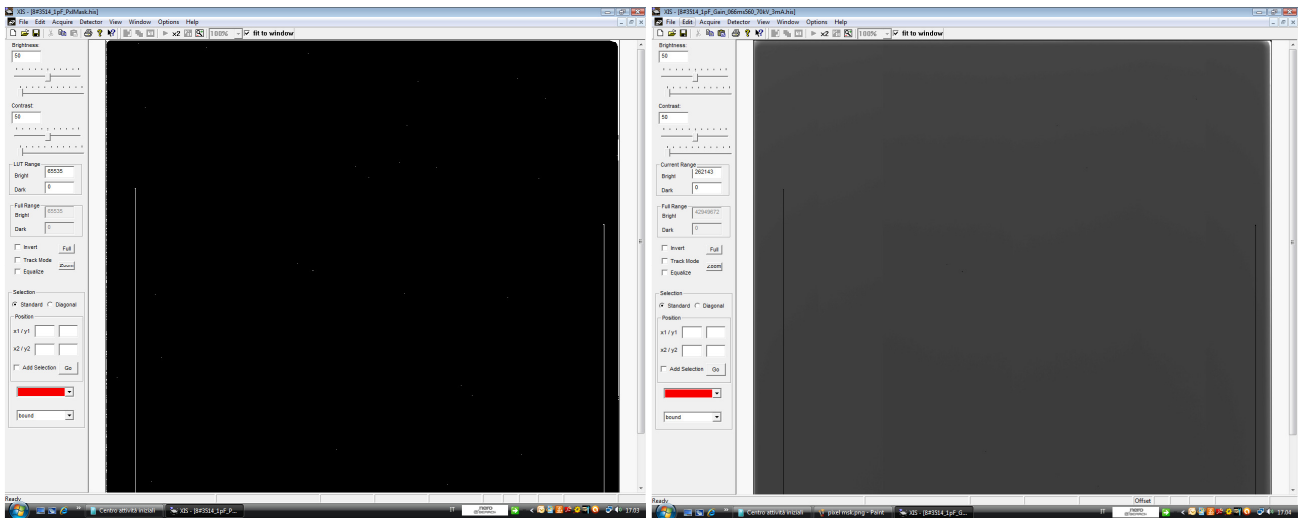


Figure 5.4. Pixel (left) and gain (gain) corrections delivered by supplier.

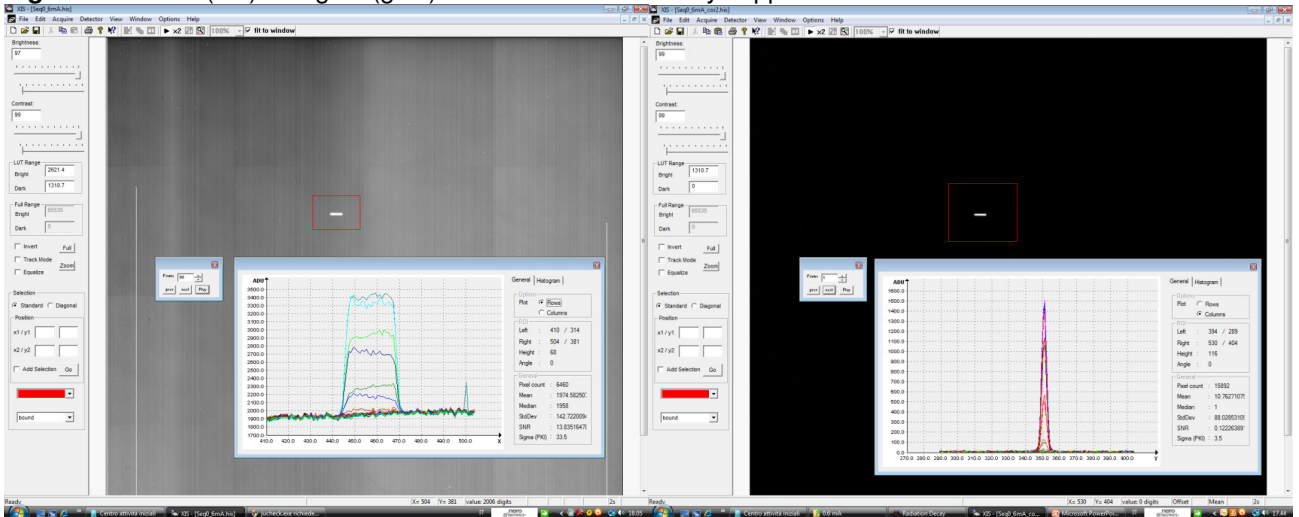


Figure 5.5. Offset (left) and pixel mask (gain) correction files created by us in the same experimental conditions of the acquired images at gain = 1 pF and integration time = 2s.

5.3 Imager characterization and calibration

5.3.1 Imager Stability

We recorded several sequences with the X-ray tube turned off to monitor the background during the operating time of the detector. Each sequence is composed by 500 frames, each of 2 s. The frames



have been corrected applying the offset and Pixel mask files. The behavior of the mean value of the background for each acquired sequence at different times (just after switching on, after 2 hours, 4 hours and finally after 8 hours) fluctuates depending on temperature and time. In fact, an important recommendation to correctly operate the imager is to refresh periodically the offset during operation.

5.3.2 Sensitivity at different collimated X-ray beam intensities

We have characterized the XRD at Larix facility using an X-ray tube that produces photons up to 120 kV. We have acquired several sequences of 150 frames by changing the X-Ray beam intensity that was collimated with a rectangular hole of area $(0.6 \times 3) \text{ mm}^2$ placed in a fixed position in front of the XRD. Each frame has an integration time of 2 s for a total acquisition time of 300 s and a gain of 1 pF. In Figure 5.6 we show the images acquired at 0.2, 0.3, 0.6 and 1.2 mA. Each image was corrected using the Pixel Mask and Offset correction files suitably created with the same experimental settings of the recorded images.

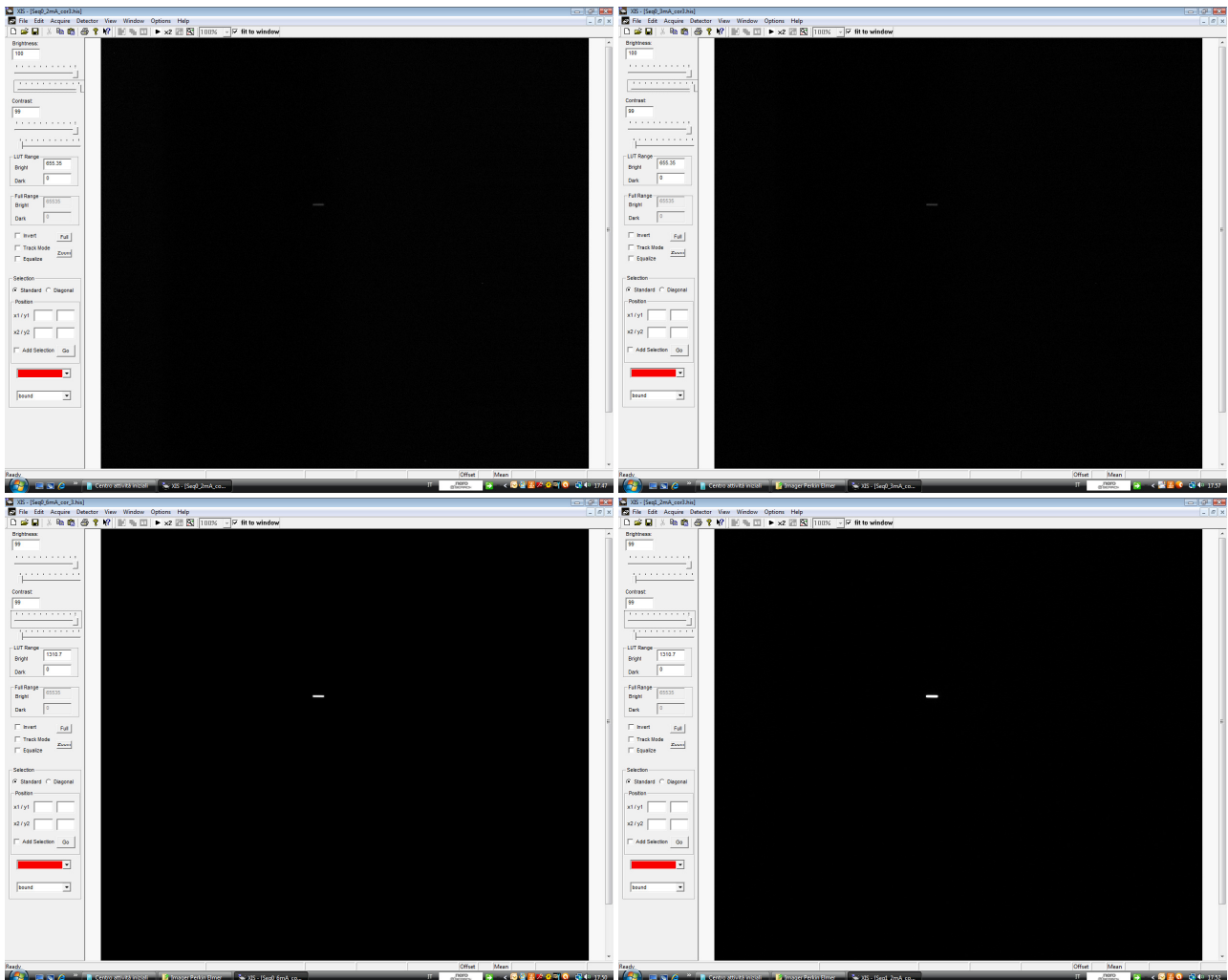


Figure 5.6. Corrected images at different intensities of the collimated X-ray beam through a rectangular hole visible near in the center of the images. In clockwise direction: 0.2, 0.3, 1.2 and 0.6 mA at 110 kV.



To verify the imager linearity we added 150 frames at different beam intensities and plot the maximum value in Analogue Digital Unit (ADU, i.e. gray levels), taken in the central region of the spot, as a function of the X-ray tube current. The graph with relative best fit is shown in Figure 5.7. The error bars are smaller than dot sizes. We can see that the behavior is linear.

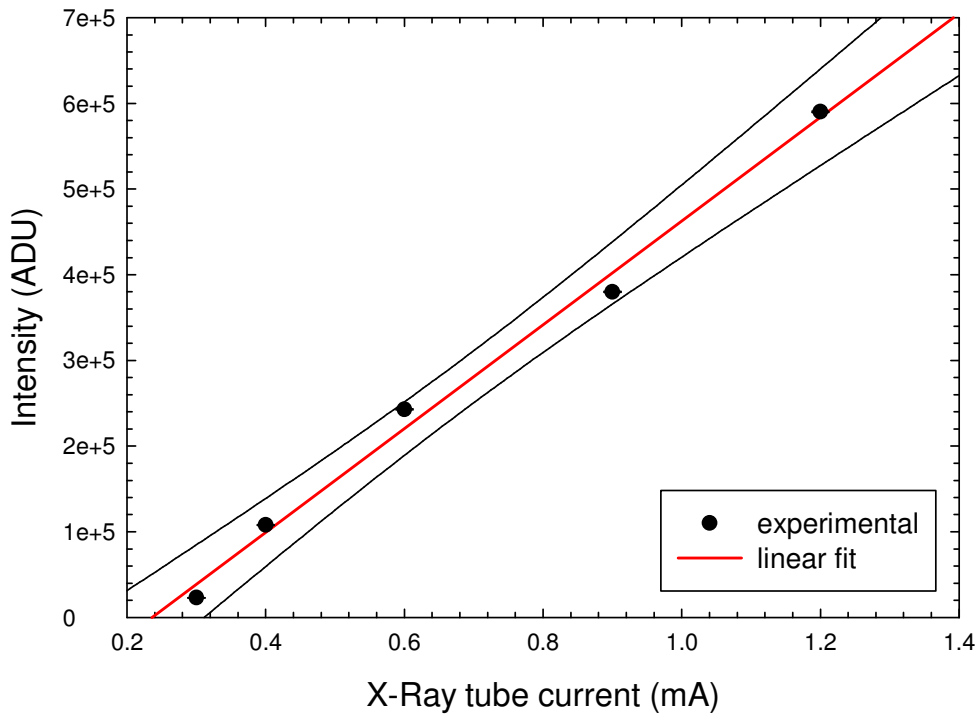


Figure 5.7. Intensity of imager detector as a function of the increasing X-Ray tube current. We have also plotted the 95% confidence band (black curves).

5.3.3 Spatial resolution

To evaluate the spatial resolution of XRD we have moved the collimated X-Ray beam from its initial position of 0.1 mm, 0.5 and 5.5 mm, where 0.1 mm corresponds to half of the detector pitch. In Figure 5.8 the images relative to the displacements are reported with the Analogue Digital Unit (gray level) profiles in the movement direction. On the upper left corner we show the image corresponding to the initial position, on the right the displacement of 0.1 mm; below on the left we report the relative position at 0.5 mm and on the right the last position (5.5 mm).

In following table we report the position of the image center in pixel and mm.

Table 5.2. Expected and measured position movements.

Expected shift (mm)	Measured shift (pixel)	Position delta (pixel)	Measured delta (mm)
0	350.5		
0.1	350	0.5	0.1
0.5	348	2.5	0.5
5.5	323	27.5	5.5

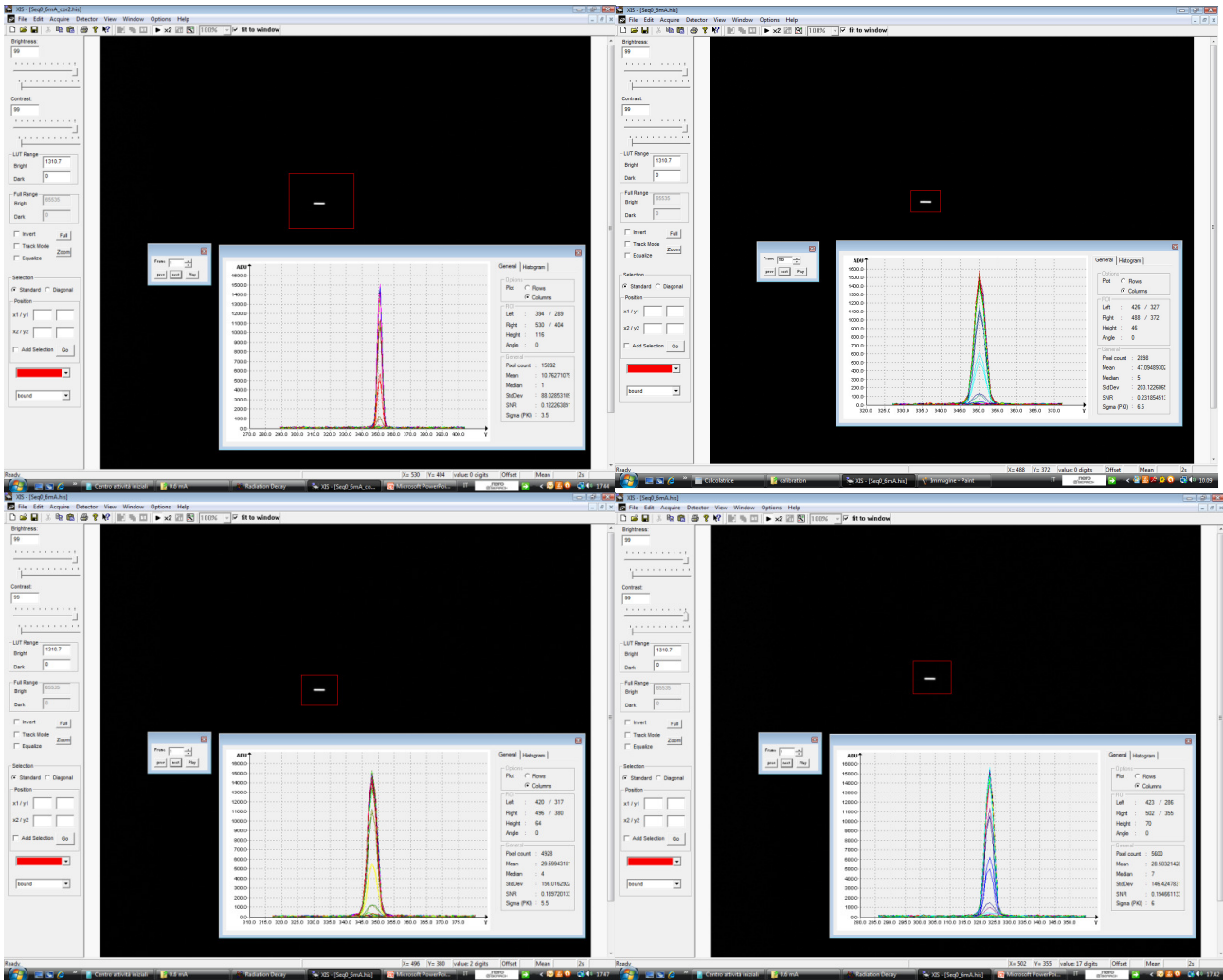


Figure 5.8. Images corrected for Offset and Pixels underperforming at different positions of the collimated X-ray beam at 110 kV and 0.6 mA.

5.3.4 Angular resolution

To evaluate the capability of the XRD of measuring angular differences we have displaced the collimated X-Ray beam from its initial position of 0.5°, 1° and 9° (see Figure 5.9).

For each acquired measurement we have fitted each pixel column with a Gaussian function and calculated the position of maximum of each distribution. Therefore, we perform a best fit of these positions with a straight line, finding the angular coefficients that we report in the following table:

Table 5.3. Expected and measured tilt angles.

Commanded Angle (°)	Measured Angle (°)	Measured Delta (°)
0	-0.48	
0.5	+0.02	0.5
1.0	0.53	1.01
9.0	8.35	8.83



We can note that the first set angle is not horizontal but presents an offset due to the imperfect alignment of the detector with the collimated beam. Taking into account this offset, the derived deltas are in good agreement with the commanded angles.

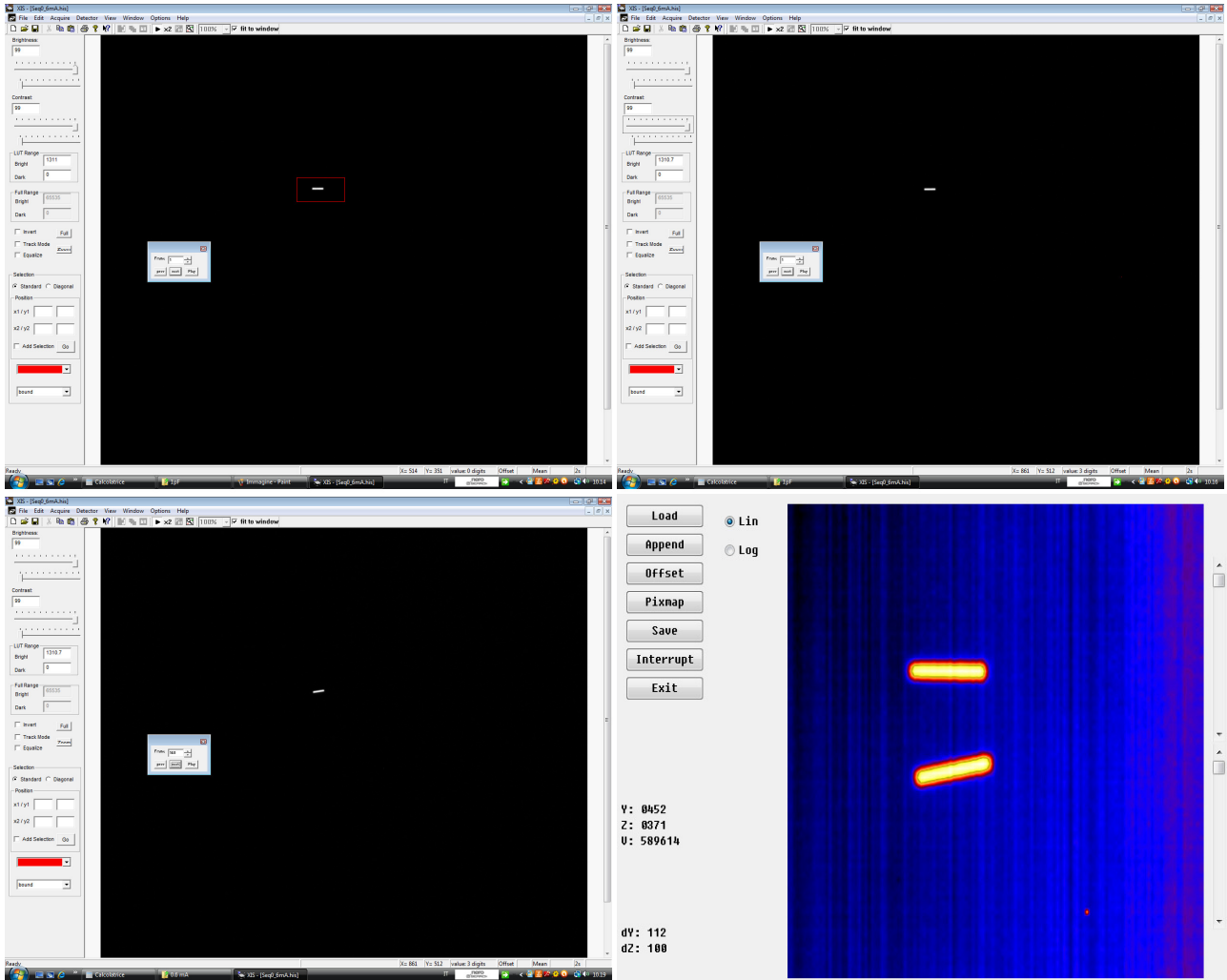


Figure 5.9. Corrected images at different angles of the collimated X-ray beam at 110 kV and 0.6 mA. The uncorrected image in the bottom right corner represents the comparison between the initial position at $\sim 0^\circ$ and 9° . The angle deviation is well visible.



6. Spectrometer Specifications

The spectrometer function is to acquire the energy spectrum before and after crystal gluing to verify that it selects the correct energy corresponding to the Bragg angle.

The spectrometer chosen to satisfy the requirements reported in [DA-03, DA-04, DA-07] is a GLP Series HPGe (High-Purity Germanium) from ORTEC, having the specifications reported in table 6.1.

Table 6.1. Spectrometer specifications.

Model and Serial Numbers	
Detector Model N.	GLP-25300/13
Cryostat Configuration	CFG-GG-GLP
Dewar Model	DWR-3.0 G
Cryogenic Information	
Dewar Capacity	3 l
Static holding time	48 hours
Detector Cool-Down Time	6 hours
Dimensions	
Detector active diameter (mm)	25
Detector sensitive depth (mm)	13
Sizes (mm ²):	325
Be Window thickness (mm)	0.254
Performance	
Energy range	3 keV - 1 MeV
Resolution FWHM at 122 keV (eV)	537 at amplifier time constant 6 μ s
Peak Shape FWTM/FWHM	1.86
Semiconductor material	P-Type High-Purity Germanium
Detector type and geometry	Planar/Low Energy Photon Spectrometer

We have carried out a complete characterization by irradiating the detector with typical radioactive sources both in Solid State Laboratory of INAF/IASF Bologna and in the Larix facility before and after mounting on the detector support as shown in Figure 6.1.

6.1 Electronics chain description

The electronics used to read the signals from the detector is composed of:

- **front – end electronics**, including the input field – effect transistor (FET) and the resistive feedback of the charge sensitive preamplifier, enclosed in the cryogenically-cooled enclosure to minimize electronic noise;
- **charge sensitive preamplifier**;
- **DSPEC - LF** Digital Gamma-Ray Spectrometer from ORTEC (see Figure 6.1, right), including the shaping amplifier and the Analogue Digital Converter. Its peculiarities are to combine small size, the latest in digital signal processing and filters, and high-speed data transfer via USB.
- **ORTEC Detector Interface Module (DIM-NEGGE)** to connect the DSPEC - LF and the detector with only a single cable. The DIM provides the **negative** bias voltage close to the detectors so that only signal and low voltage power are carried in the cable.

The detector system is equipped with a temperature-sensing element located in the cryogenic vacuum enclosure in order to automatically shut off the HV power supply if the detector temperature begins to increase.



The DSPEC LF is connected to PC via the high-speed USB port and it was shipped with two AC/DC power supplies, a through-ground model and a floating – ground model. If ground loops are present (these effects are identified by elevated dead time, >1% without radioactive sources near the detector) it recommends trying both the supplies to determine which could resolve the issue.

The DSPEC LF has a LCD display for monitoring the current real and live time (RT and LT), the real time and live time presets (RTP and LTP), the dead time percentage and input count rate in counts per second (DT and ICR), the stabilizer settings, the current HV value and status (ON/OFF) and the shutdown mode. Figure 6.2 shows the display for the DSPEC-LF connected at our HPGe with the ID number for this instrument as set by the MCB Configuration program, the firmware version and the USB connection on the last line.

The DSPEC LF is completely software controlled by MCB Properties dialog (see section 6.2), that includes all the controls of the instrument summarized in following subsections.

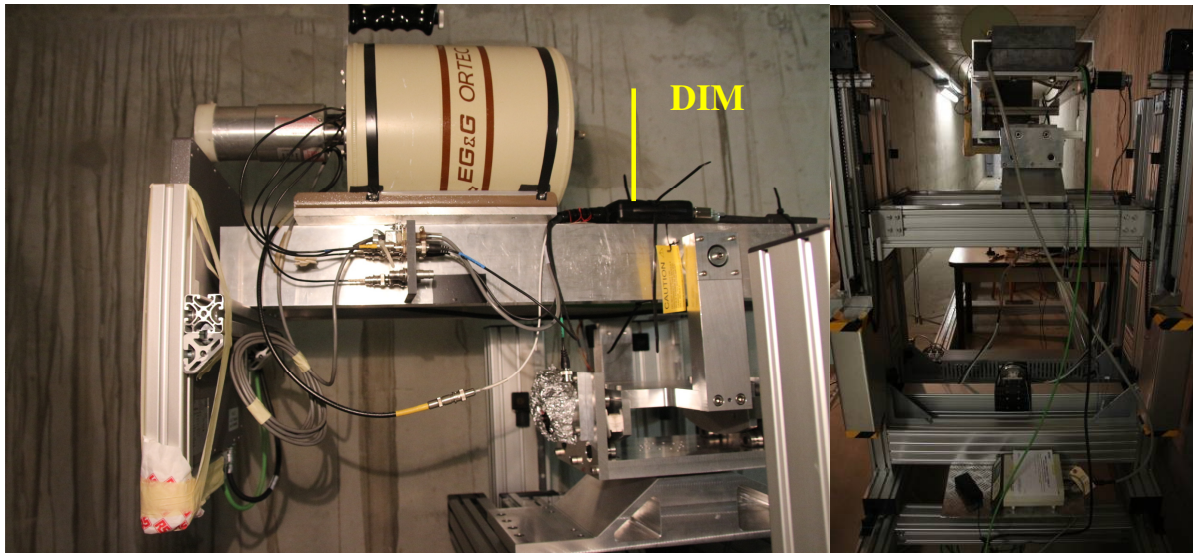


Figure 6.1. HPGe detector mounted at Larix facility with its Detector Interface module (DIM).

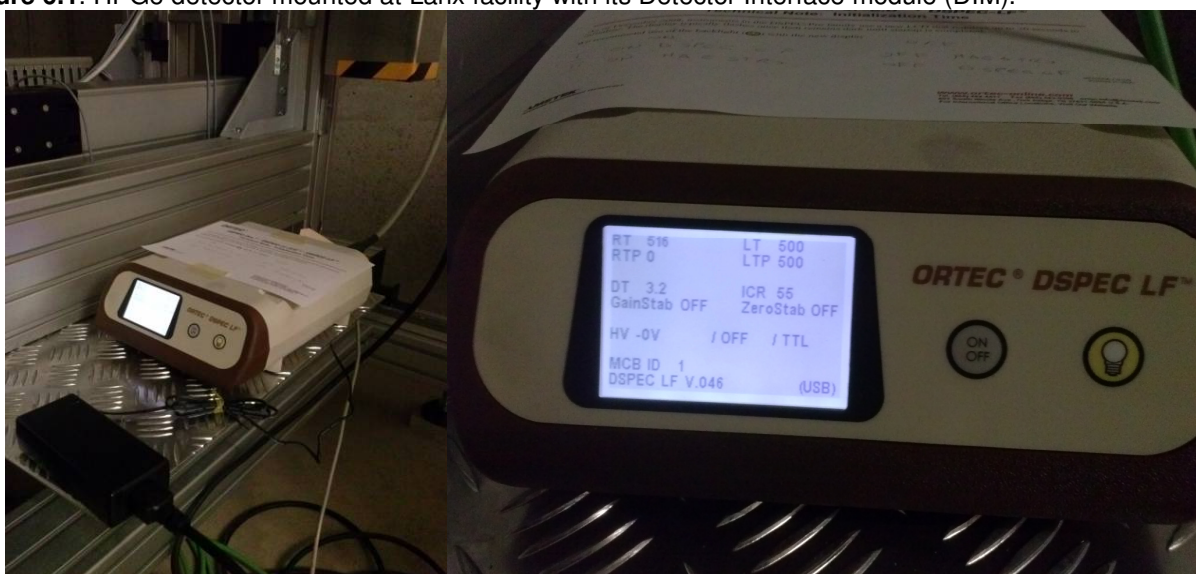


Figure 6.2. The DSPEC-LF electronics.



6.1.1 Amplifier and Amplifier 2

The Amplifier tab contains the controls for the Gain (coarse and fine to cover a amplification range from 0.25 to 32), Baseline restore, used Preamplifier type, Amplifier Input polarity and Optimize. The Amplifier 2 tab allows to set the shaping time value from 0.8 to 23 μ s, in steps of 0.2 μ s, and to perform a pole zero at a specified rise time (see Figure 6.3).

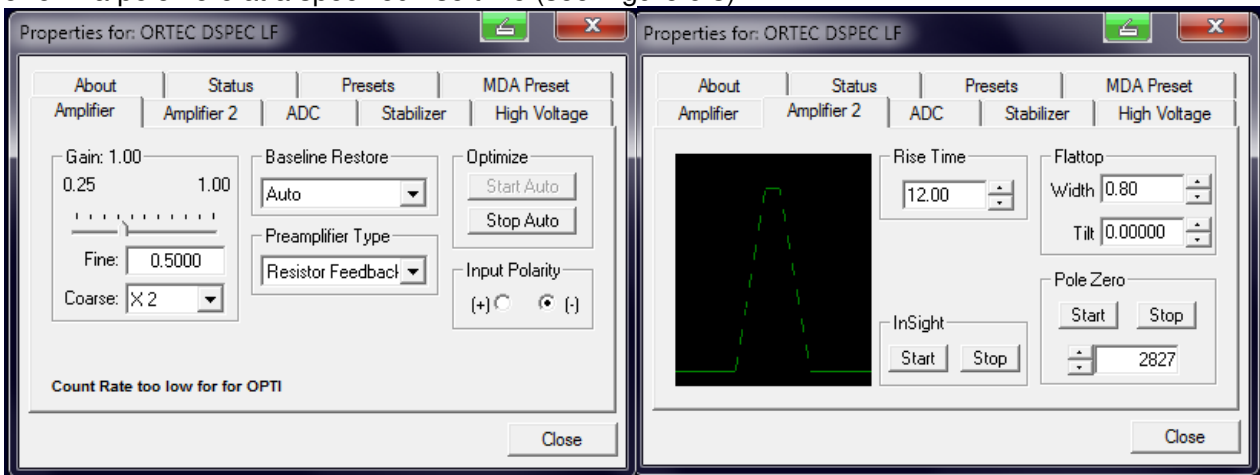


Figure 6.3. Amplifier and Amplifier 2 tabs.

We have optimized the spectroscopic response of DSPEC - LF using the START AUTO button of the Optimize feature to automatically choose the best pole zero and flattop tilting, because the DSPEC - LF is equipped with automatic pole zero and flattop logic.

The detector was been connected in its configuration and for optimizing takes place we have illuminated it with a radioactive source of ^{241}Am so that the count rate induces a dead time of $\sim 5\%$. During optimizing, pole zeroes are performed for several rise time values and the DSPEC - LF is cycled through all the rise times for determining the optimum tilt values. These values are stored in DSPEC - LF. In Figure 6.4 the comparison between the spectrum acquired before and after optimizing at 12 μ s is reported. The FWHM is 566 eV before optimizing and 539 eV after this process.

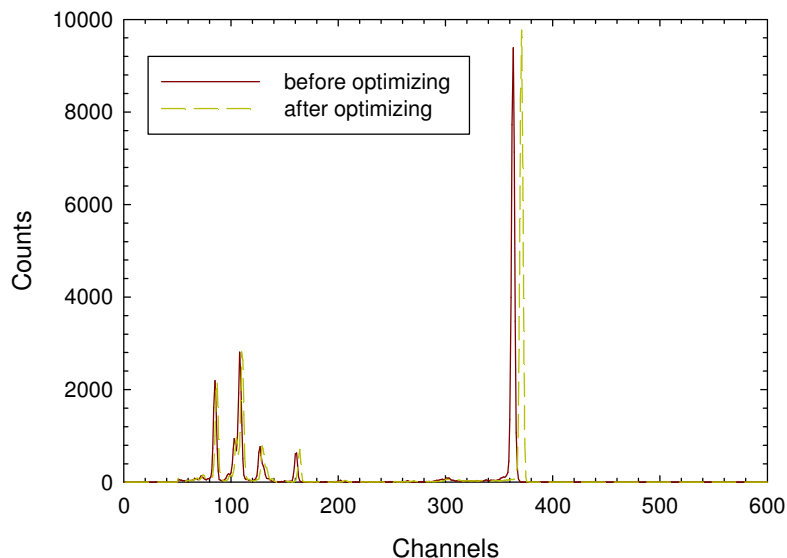


Figure 6.4. Comparison between the spectra acquired before and after optimizing at 12 μ s.



It is worth noting that the value of the rise time in DSPEC – LF is approximately equivalent to twice the integration time set on a typical analog spectroscopic amplifier. A value of the rise time parameter of 12 μ s corresponds to 6 in a conventional amplifier.

6.1.2 ADC

The tab illustrated in Figure 6.5 reports the ADC controls: Conversion Gain, Lower Level Discriminator, Upper Level Discriminator and Gate. Furthermore the actual real time, live time and count rate are monitored at the bottom of the dialog box.

The system conversion gain is software controlled from 512 to 16384 channels; practically it selects the maximum number of channels in the spectrum. Lower Level Discriminator sets in channels the minimum signal amplitude which will be stored. It is a hard cutoff of data in channels below the LLD setting. Upper Level Discriminator stores the highest amplitude of the pulses in channels.

The gate function is selectable as off (no gating is performed, equivalent to process all detector signals), coincidence (a gating input signal must be present for the event conversion) or anticoincidence (the gating input signal must not be present for the signal conversion).

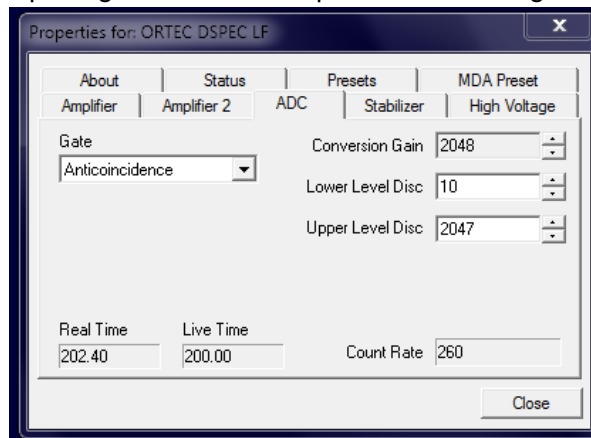


Figure 6.5. ADC tab.

6.1.3 High Voltage

The High Voltage tab (Figure 6.6) allows switching on/off the bias voltage, to set (target) and monitor (actual) the bias voltage. In addition it is possible to choose the shutdown mode. The polarity is determined by the DIM.

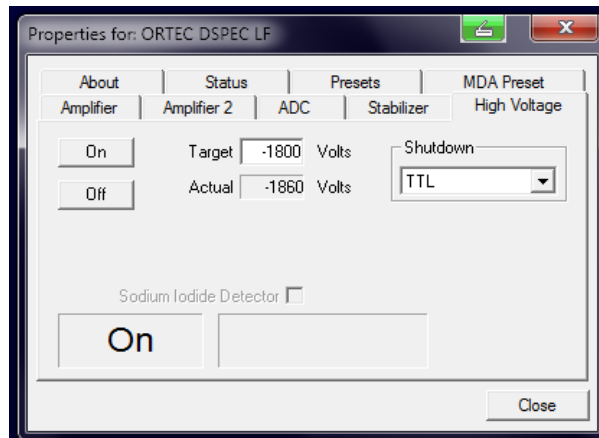


Figure 6.6. High Voltage tab.

6.1.4 Status

This tab displays simultaneously 6 of 18 values monitored at all time (Figure 6.7). The selected values can be changed at any time. Two kinds of values are presented: OK or ERR and numeric value. The parameters displayed are: Detector state of health, DIM +24V state of health, DIM +12V state of health, DIM -24V state of health, DIM -12V state of health, detector temperature state of health, high voltage state of health, shutdown state of health, preamplifier overload state of health, security state of health, power state of health, +24 Volts, +12 Volts, -24 Volts, -12 Volts, high voltage.

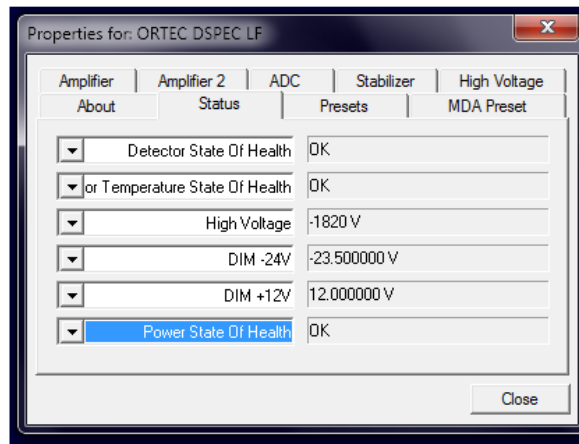


Figure 6.7. Status tab.

6.1.5 Presets

Figure 6.8 shows the parameters that can be set to acquire automatically a measurement: real time, live time, counts in the ROI peak, counts in the ROI integral. These parameters must be set when the detector is not acquiring data because during acquisition the preset fields are inactive.

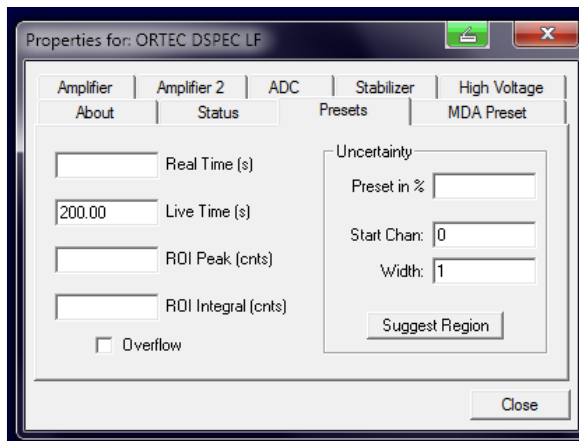


Figure 6.8. Presets tab.

6.2 Software description

The software utilized to record the spectra is a commercial S/W, MAESTRO® MCA Emulator from Ortec, which allows managing the DSPEC – LF controls by means of the Multi Channel Buffer Properties, in the Acquire menu. The main functions of the Multi Channel Analyzer are the acquisition control (Start/Stop/Clear), the spectra storage (Save/Import/Export) and analysis (Energy calibration/Peak Search/Peak information/Compare/Sum/Strip/etc).



6.3 Characterization and calibration at IASF Bologna laboratory

6.3.1 Characterization as a function of the bias voltage and amplifier shaping time

We have carried out a characterization as a function of the bias voltage applied to fully deplete the detector and another one as a function of the shaping time to obtain the value corresponding to the best energy resolution. Both studies are performed by irradiating the HPGe detector with a collimated ^{57}Co source that presents three main lines at 14.41, 122.06 and 136.47 keV and an amplifier gain of 1. We waited 600 s before increasing each voltage step to stabilize the electric field.

In Figure 6.9 we illustrate the spectra acquired from -1500V to -2000V, that is the operating bias voltage reported in the HPGe data sheet, with a shaping time of 6 μs for a live time of 900 s. The centroids and the FWHMs calculated at 122 keV are reported in table 6.2.

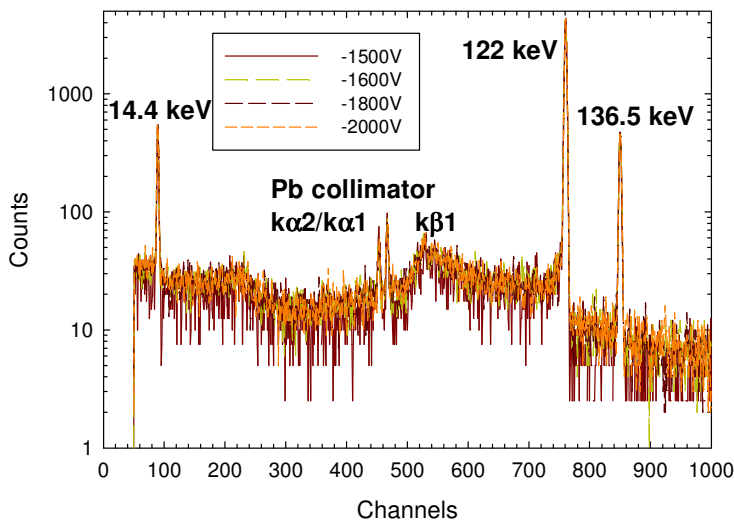


Table 6.2. Centroid channels and energy resolutions (FWHM) at 122 keV for several high voltage.

Bias (V)	Centroid at 122 keV (channels)	FWHM at 122 keV (eV)
-1500	758.89	576
-1600	758.90	574
-1800	758.96	563
-2000	758.95	565

Figure 6.9. ^{57}Co spectra acquired at different high voltage.

We can note by analyzing data that the peak centroid is about at the same channel but the energy resolution (FWHM) is lower at -1800V, as a consequence we choose this value as operating bias voltage. After setting this high voltage we have changed the shaping time from 4 μs to 8 μs to determine the optimum value. The spectra are shown in Fig. 6.10 and the analysis results in table 6.3.

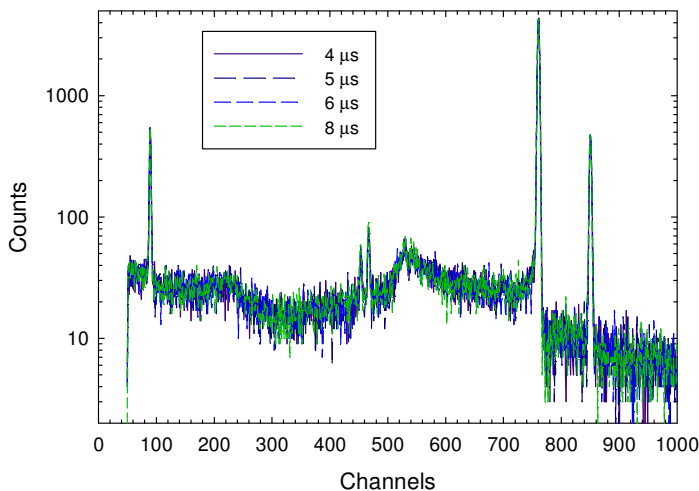


Table 6.3. Centroids and energy resolutions (FWHM) at 122 keV for several shaping time. The bias voltage is -1800V and the live time 900s.

S.T. (μs)	Centroid at 122 keV (channels)	FWHM at 122 keV (eV)
4	758.91	571
5	758.92	569
6	758.96	563
8	758.89	577

Figure 6.10. ^{57}Co spectra acquired at several amplifier shaping time.

The behavior of the centroid channel è stable and the FWHM presents a minimum at 6 μ s, as we can see in the following figure:

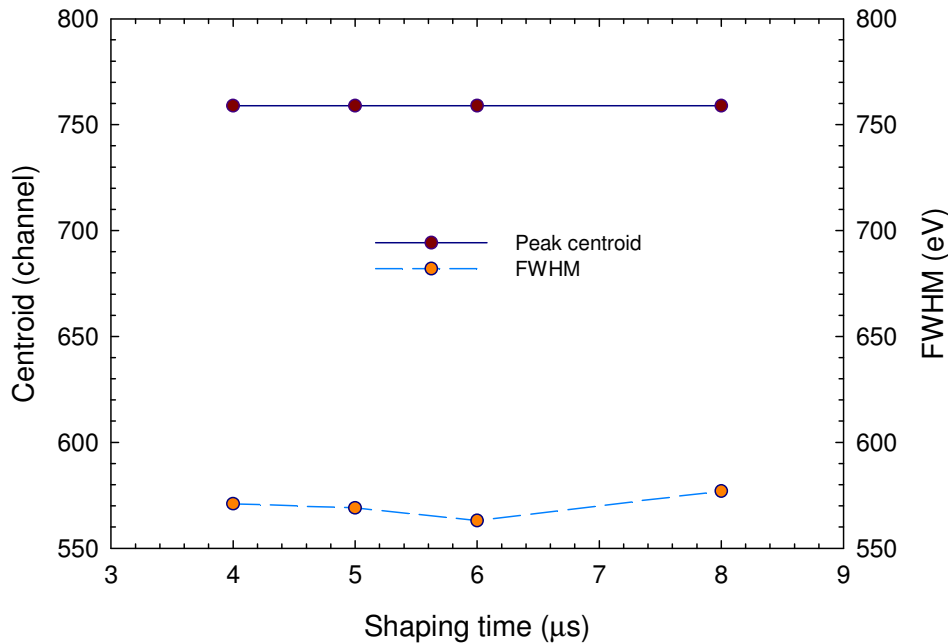


Figure 6.11. Peak centroid and energy resolution behavior at 122 keV.

We have also acquired the spectrum of background without irradiating the detector with the radioactive sources, but as the background counts are not significant, we have not subtracted the background spectrum.

6.3.2 Characterization as a function of the energy

We have recorded a spectrum of the ^{241}Am collimated source (lines at 13.95, 17.75, 26.34 and 59.54 keV) and ^{109}Cd (lines at 22.16, 24.94 and 88.04 keV) by setting the operating values found in the previous section: -1800V for the high voltage and 6 μ s for the amplifier shaping time. In addition we have acquired a ^{57}Co spectrum, decreasing the LLD in order to evaluate the low energy threshold. These spectra are displayed in Figure 6.12 on the left. The energy resolutions are reported in table 6.4.

Table 6.4. Energy resolutions (FWHM) as a function of the energy.

Energy (keV)	FWHM (eV)
6.4	168
59.54	488
88	528
122	570

We have also acquired a ^{133}Ba spectrum, representative of the energy band of the Laue lens at gain 0.5. This spectrum is reported in Figure 6.12 on the right with the ^{241}Am and ^{57}Co spectra at the same gain.

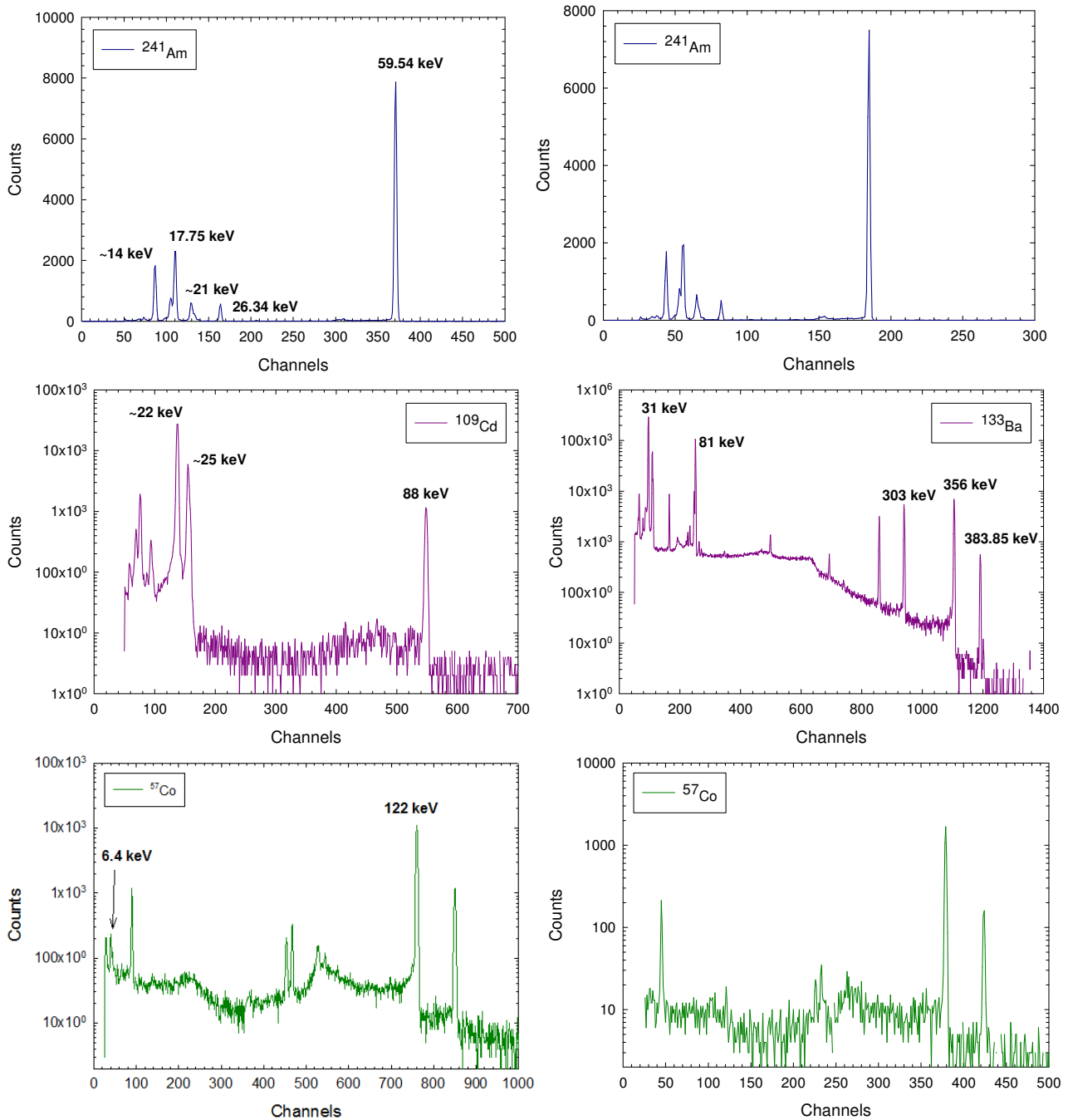


Figure 6.12. Spectra acquired at different energies at gain=1 on the left and at gain = 0.5 on the right.

In figure 6.13 we illustrate the behavior of the centroid channel of the measured peaks as a function of the energy at 6.4, 14.41, 59.54, 88, 122 keV at gain 1 on the left and at 59.54, 81, 122, 303 and 356 keV at gain 0.5 on the right. We can note that the detection system is linear over the energy range of the Laue Lens. Blue circle are the experimental measurements, while the red line represent the best fit.

The FWHM in table 6.4 is reported as a function of the energy in Figure 6.14, where we can see that it is almost proportional to the square root of the gamma ray photon energy being the best fit slope equal to 0.45. In blue the experimental points are reported and in red the linear fit.

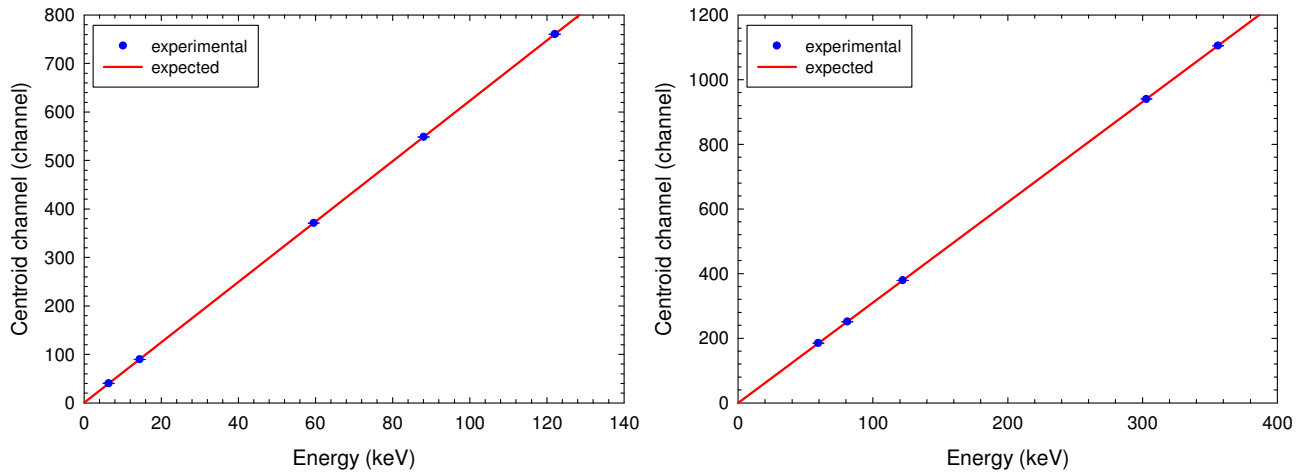


Figure 6.13. Linearity of the detection system composed of the sensor HPGe and DSPEC-LF at gain 1 (left) and 0.5 (right). The experimental measurements are reported in blue and the linear fit in red. The error bars are smaller than the point sizes.

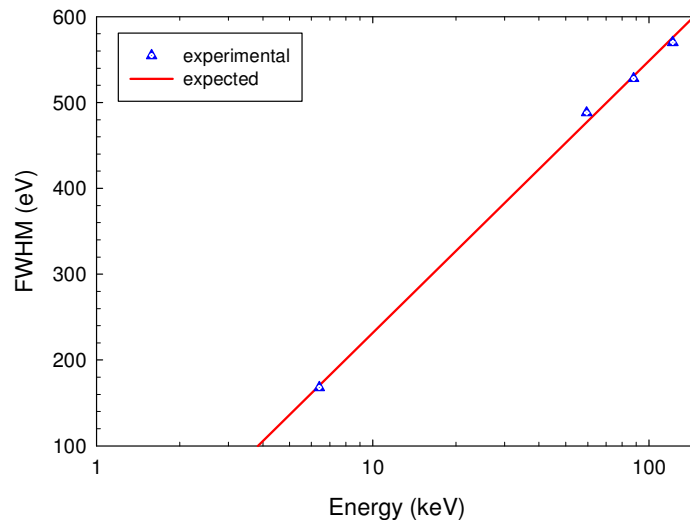


Figure 6.14. Variation of the FWHM as a function of the gamma ray energy at gain 1. Blue triangles are the experimental measurements, while the red line represent the best fit.

We have changed the power supply verifying that the detector performances are unaffected at our laboratory that is an environment without ground loops. The comparison between two spectra acquired in the same experimental conditions, by irradiating the detector both with and without radioactive sources, is reported in Figure 6.15.

We can note that the spectra overlap fully, and as a consequence we can infer that at IASF Bologna laboratory both power supplies work well.

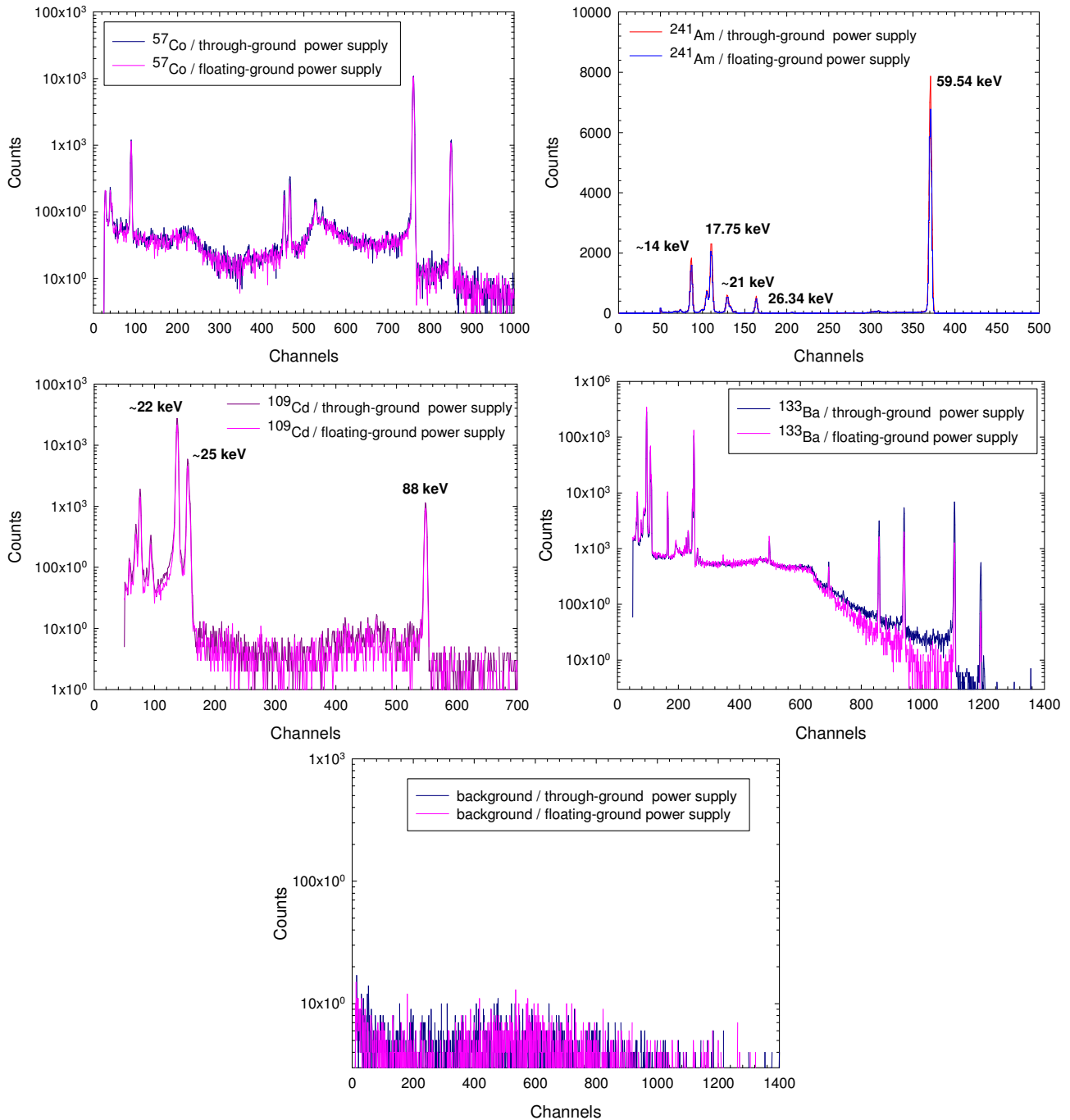


Figure 6.15. Comparison of two spectra acquired with the provided power supplies, a through-ground and floating-ground model, by illuminating the detector with ^{57}Co , ^{241}Am , ^{109}Cd and ^{133}Ba . The last graph below shows the comparison of the background spectra recorded using two power supplies.



6.4 Characterization at Larix facility

6.4.1 Characterization as a function of the bias voltage and amplifier shaping time

We have repeated the characterizations as a function of the bias voltage and the amplifier shaping time to confirm the values determined previously for these parameters after assembling both imager and HPGE detector on the metallic structure support. The mounting was optimized taking in account the microphonic behaviour of the detector, the ground loops resulting when several electronic components are grounded in different places (causing slightly differing near-ground potentials), and signal pickup occurring. We have tested both the power supplies and chosen the through-ground model because it causes very low counts. We have repeated the optimization procedure in the final configuration. The results of spectra analyses acquired at 59.54 keV are reported below.

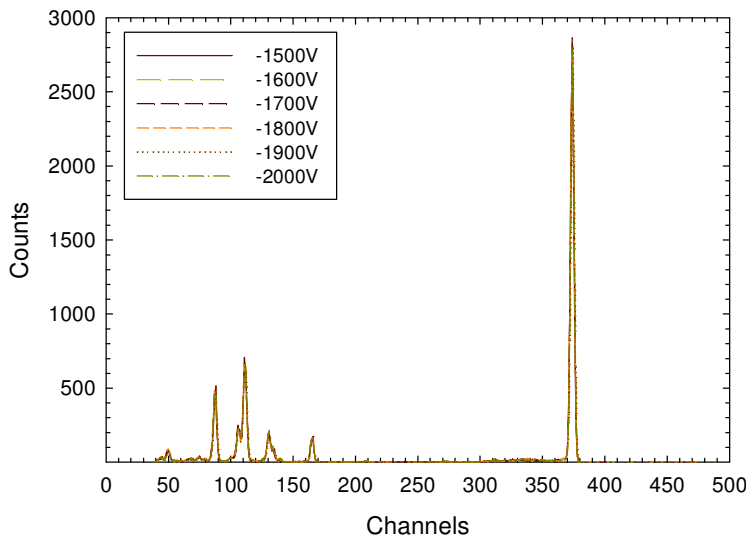


Table 6.5. Centroid channels and energy resolutions (FWHM) at 59.54 keV for several bias voltage.

Bias (V)	Centroid at 59.54 keV (channels)	FWHM at 59.54 keV (eV)
-1500	372.43	478
-1600	372.45	469
-1700	372.44	460
-1800	372.45	483
-1900	372.46	464
-2000	372.47	465

Figure 6.16. ²⁴¹Am spectra acquired at different bias voltage at Larix facility.

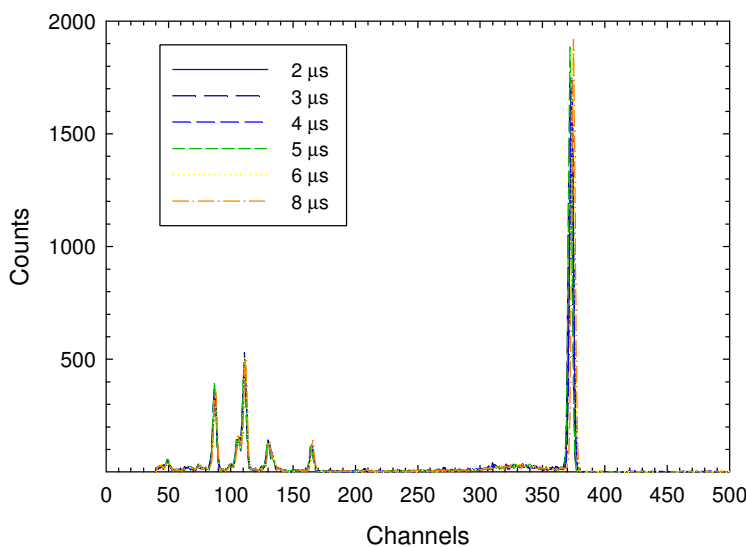


Table 6.6. Centroids and energy resolutions (FWHM) at 59.54 keV for several shaping time. The bias voltage is -1700V and the live time 100s.

S.T. (μs)	Centroid at 59.54 keV (channels)	FWHM at 59.54 keV (eV)
2	371.88	570
3	371.26	555
4	371.96	535
5	371.62	502
6	372.52	451
8	373.42	485

Figure 6.17. ²⁴¹Am spectra acquired at several amplifier shaping time at Larix facility.

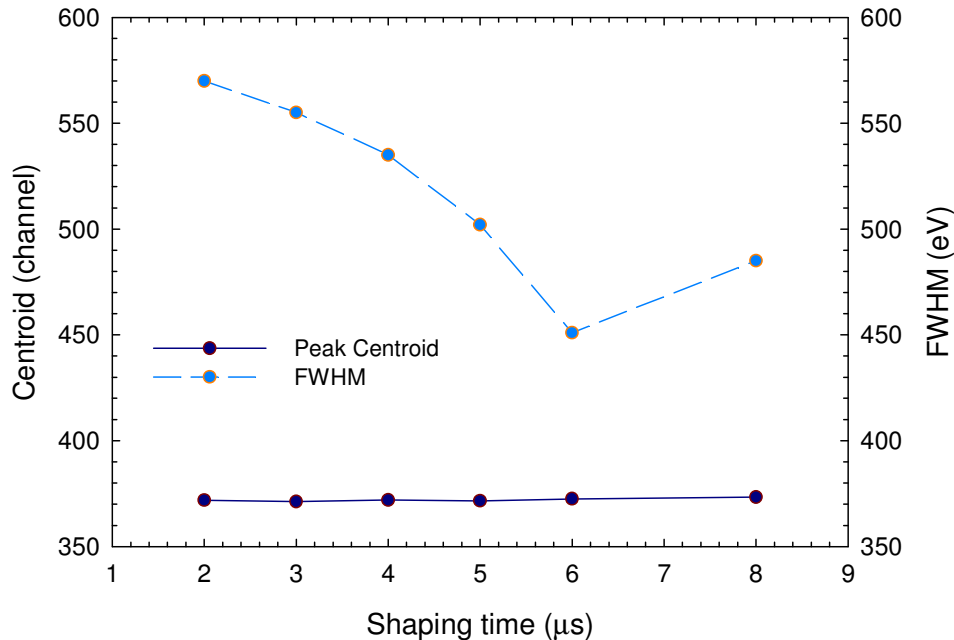


Figure 6.18. Peak centroid and energy resolution behavior at 59.54 keV.

We can conclude that at Larix facility, after integrating the HPGe detector on the structure of supporting, the determined operating values of the bias voltage and amplifier shaping time are -1700V and 6 μs.

6.4.2 Characterization as a function of the energy

In the final setup, ready to start the operations to glue the crystals, we have performed the energy characterization both at gain = 1 and at gain = 0.5. The results are illustrated in the following figures and tables.

Table 6.7. Energy resolution (FWHM) as a function of the energy obtained by acquiring measurements in the final experimental setup at Larix facility.

Energy (keV)	FWHM (eV)
59.54	478
81	503
122	563
303	783

We can infer that both at IASF Bologna laboratory and at Larix facility the energy resolution at 122 keV is in accordance to the value of 540 eV measured by the supplier.

We show also in Figure 6.20 a zoom of the ^{133}Ba spectrum, where we can see in detail the different peaks detected from the HPGe.

In Figure 6.21 the good linearity for both gains over the entire energy range of the Laue lens is reported.

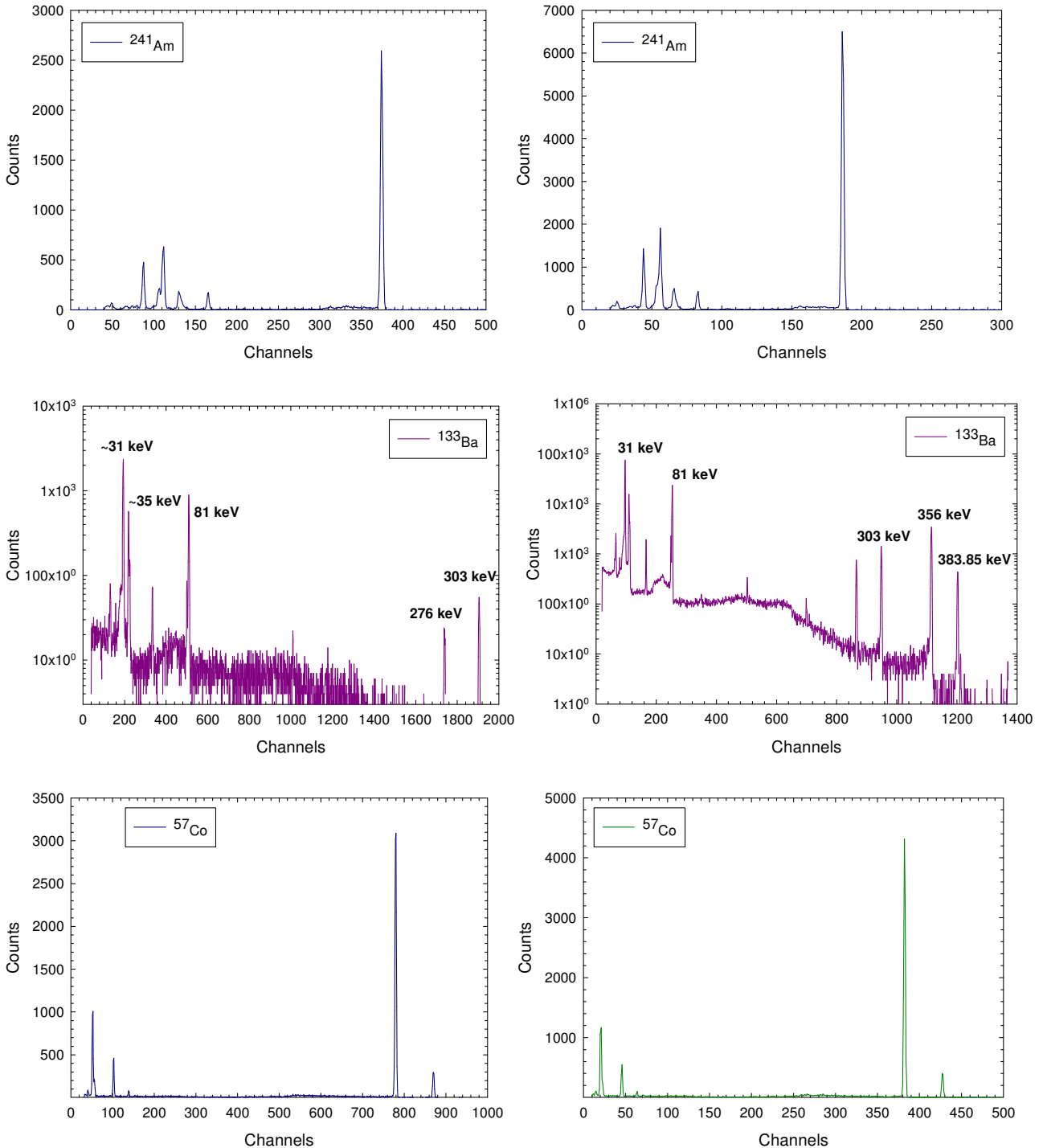


Figure 6.19. Spectra acquired at different energies at gain=1 on the left and at gain = 0.5 on the right.

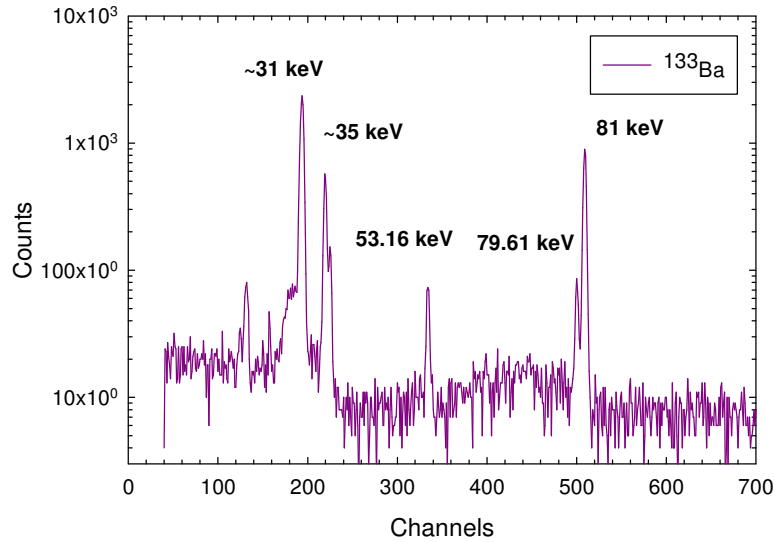


Figure 6.20. Zoomed region of the ^{133}Ba spectrum acquired at gain=1.

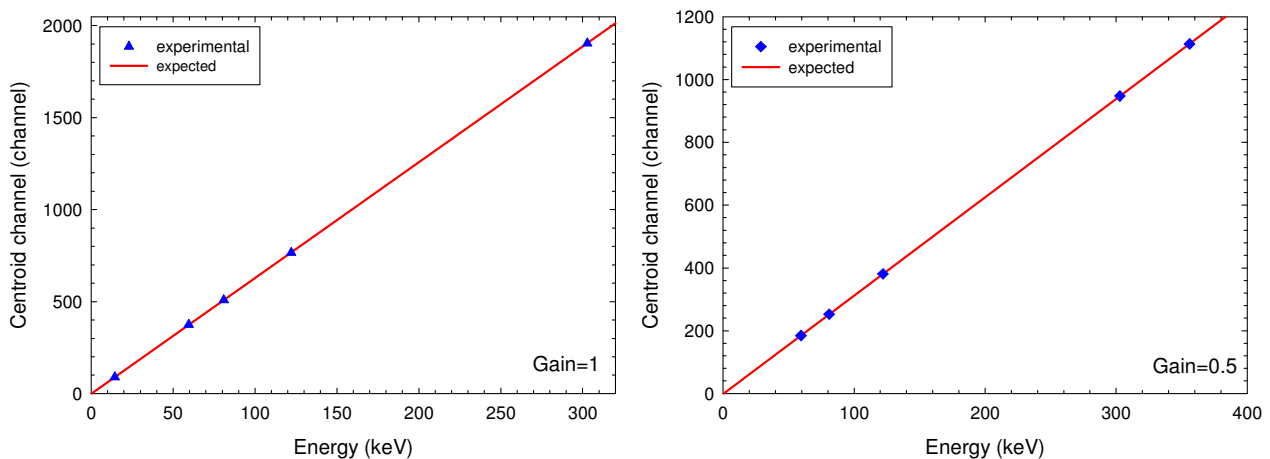


Figure 6.21. Linearity at gain 1 (left) and 0.5 (right). The experimental measurements are reported in blue and the linear fit in red.

6.4.3 Comparison between DSPEC-LF and Standard Nuclear Instrumentation Systems

The DSPEC-LF performance has been compared with that obtained from a standard electronic chain, composed of main shaping amplifier (Silena 7611), linear gate and stretcher (Ortec 542), ADC and MCA, as displayed in the schematic drawing of Figure 6.22. The HPGe detector has been illuminated with different radioactive sources and the output signal has been connected at the same time with the DSPEC-LF and the standard chain. The amplifier gains were adjusted so that the centroids of the main peaks were approximately at the same channel.

The spectra have been acquired setting the same operating parameters: bias voltage, shaping time of the amplifiers and live time of MCAs utilized.

Figure 6.23 compares the spectra of both systems by irradiating with ^{241}Am , ^{109}Cd , ^{57}Co , while in table 6.8 the FWHM values are reported.

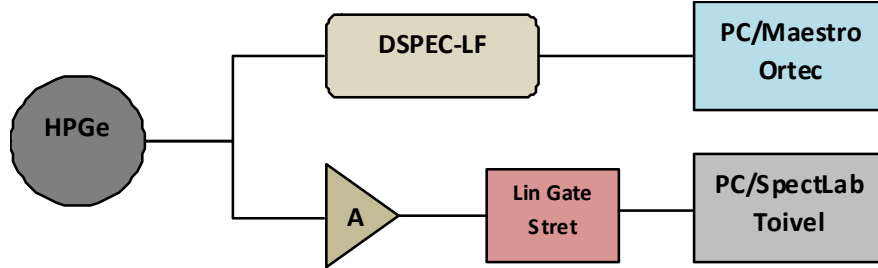


Figure 6.22. Block diagram of the configuration adopted to acquire in parallel with both systems.

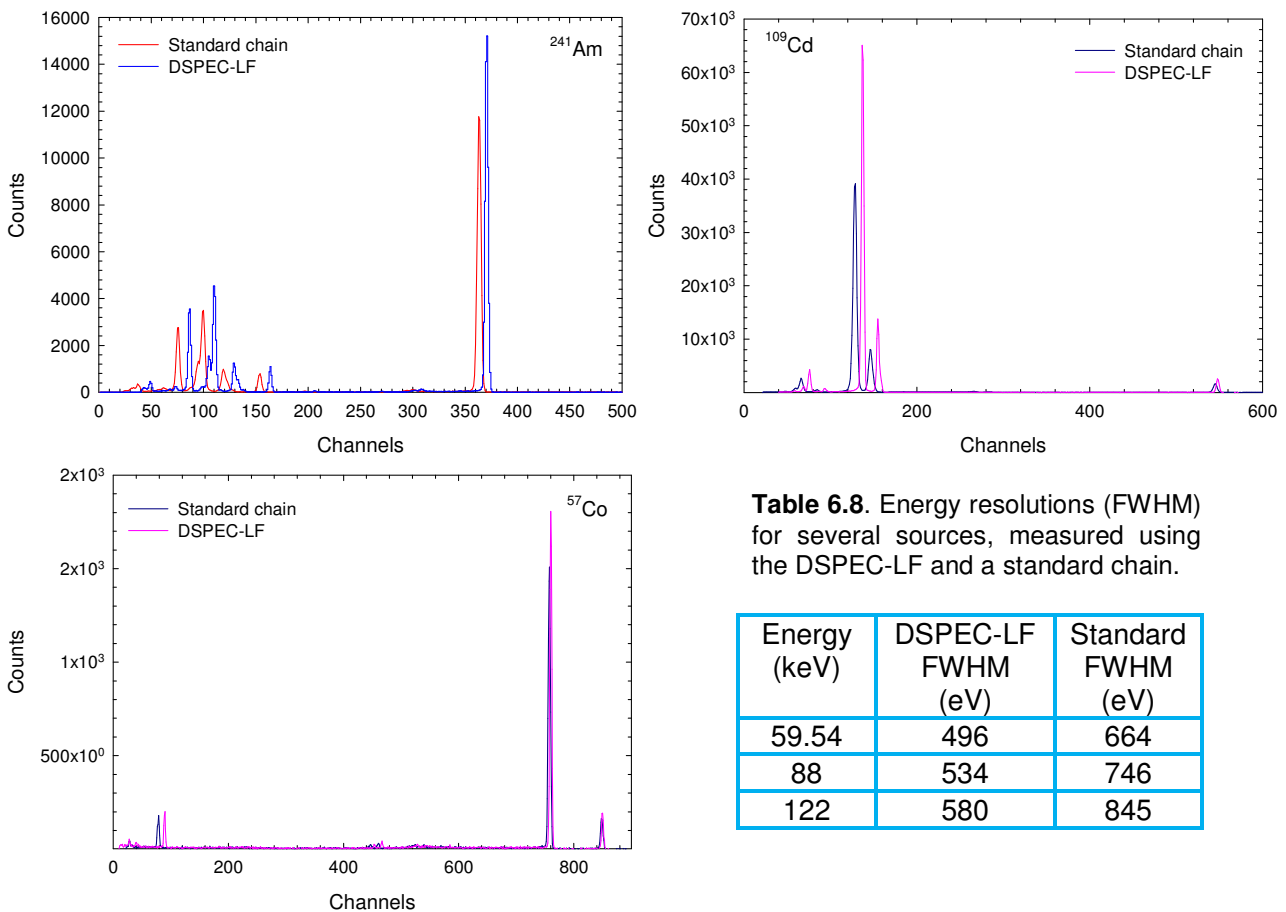


Table 6.8. Energy resolutions (FWHM) for several sources, measured using the DSPEC-LF and a standard chain.

Energy (keV)	DSPEC-LF FWHM (eV)	Standard FWHM (eV)
59.54	496	664
88	534	746
122	580	845

Figure 6.23. Comparison between the spectra acquired in parallel with the DSPEC-LF and a standard chain.

We can conclude that the performance obtained with DSPEC-LF system is better with respect to that of the standard chain. The energy resolution calculated at 59.54 keV is 664 eV instead of 496 eV recording a ^{241}Am spectrum in parallel respectively with a typical electronic chain and the DSPEC-LF.

6.4.4 Instruments interference

We have also acquired a measurement with the imager turned on to verify that two instruments do not affect with each other. As it can see in the following figure this effect does not occur in our environment, after optimizing the setup.

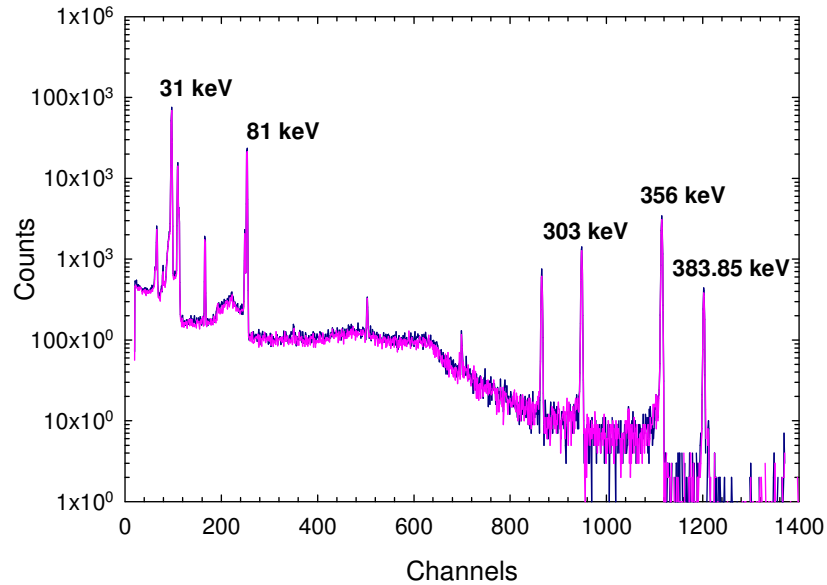


Figure 6.24. Spectra comparison acquired switching on and off the digital X-ray Detector.

6.4.5 Requirement on the energy resolution

To verify the required energy resolution of 160 eV at 80 keV we have acquired several measurements with ^{133}Ba and fitted the peak at 81 keV with a Gaussian distribution. The histogram of the centroid channels is fitted with the Gaussian function, obtaining a mean value of 252.54 channels, relative to 81 keV, and a deviation standard of 0.017 channels corresponding to 6 eV. We can conclude that the requirement is complied. The channel distribution (in dark) and the Gaussian fit (in red) are displayed in Figure 6.25.

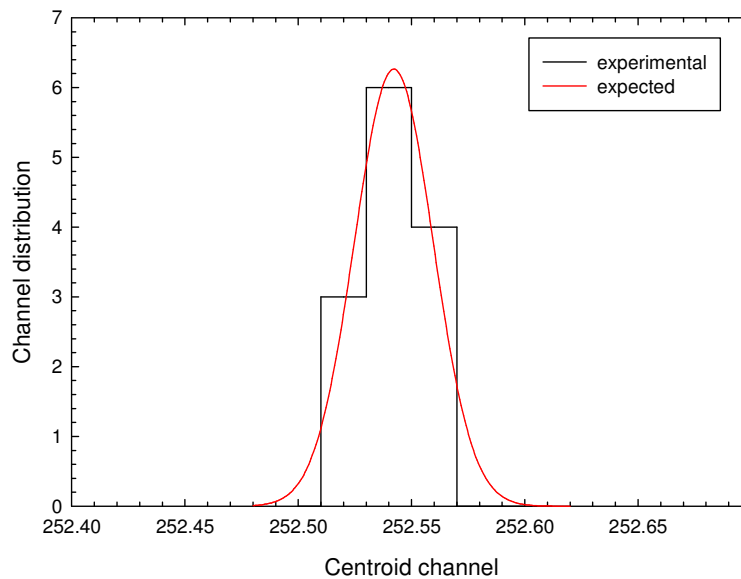


Figure 6.25. Channel distribution at 81 keV for a significant sample (15) of measurements.



6.4.6 Spectrometer Stability

We have verified both at IASF Bologna laboratory (Figure 6.26, top) and at Larix facility (Figure 6.26, bottom) that the spectrometer and relative readout system are stable, behavior confirmed by acquiring several spectra in the same experimental conditions but at different times and after restoring some parameters as the shaping time and gain. In following figure an example is shown, in which we can see that the differences in the spectra are statistical.

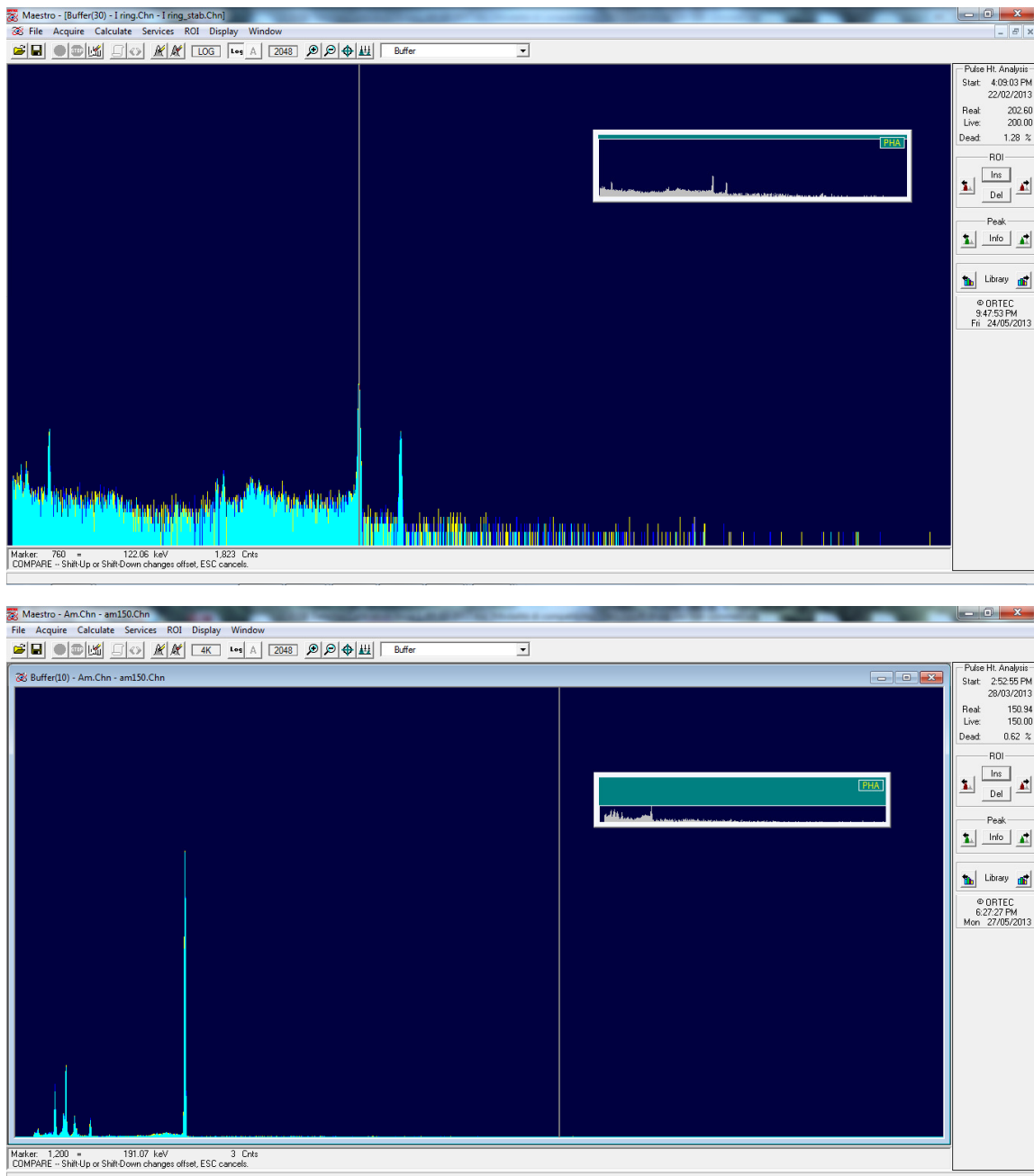


Figure 6.26. System stability at IASF Bologna laboratory (top) and at Larix facility (bottom).



6.4.7 Background

Furthermore, we have studied and monitored the background level in laboratory and inside the X-ray facility tunnel.

Figure 6.27 illustrate the background at IASF laboratory acquired in 900 s when the detector is operative during the same day at different time (left) and after 24 hours (right).

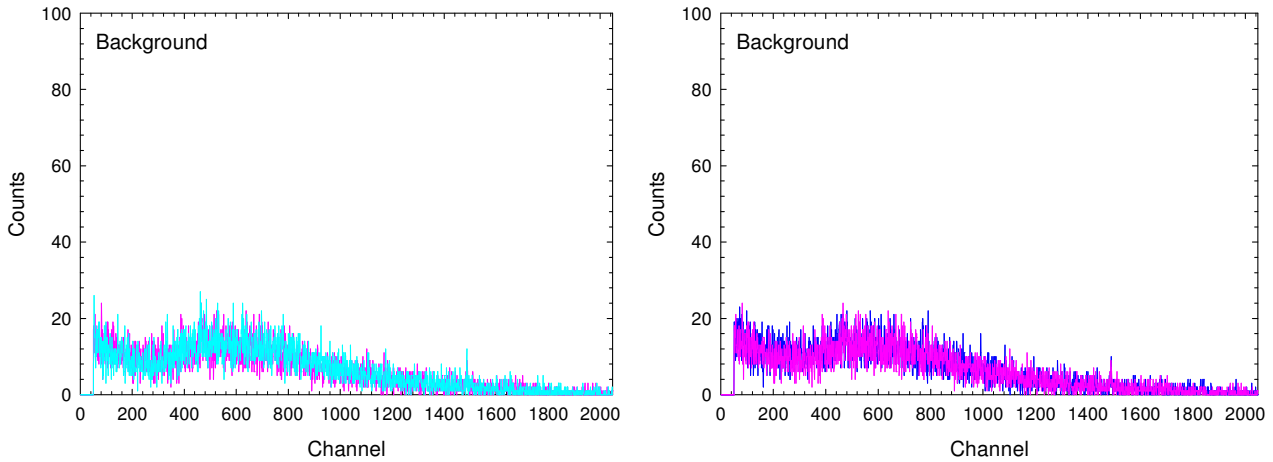


Figure 6.27. Background level at IASF Bologna laboratory when the detector is operative during the same day (left) and after 24 hours (right).

In Figure 6.28 we show the background at Ferrara facility acquired in 100 s during the same day at three different times (left) and after 15 days (right) with an acquisition time of 150 s.

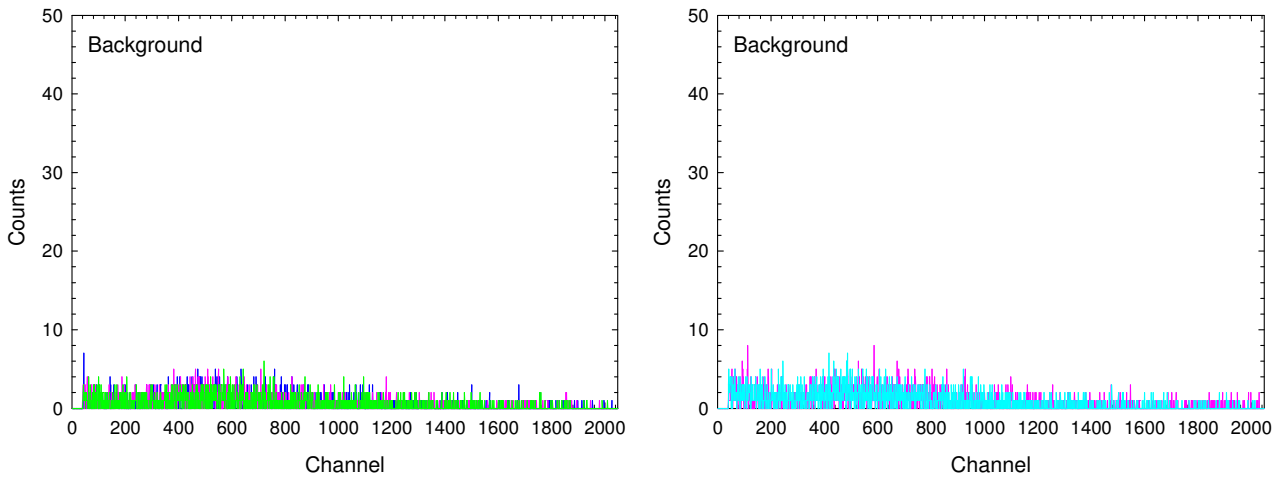


Figure 6.28. Background level inside the tunnel when the detector is operative during the same day (left) and after 15 days.

In Figure 6.29 we report the comparison of the background acquired at Ferrara facility with one recorded at IASF Bologna laboratory in 100 s (left) and in 300 s (right).



We can conclude that the background is stable and lower at LARIX facility with respect to one recorded at IASF Bologna laboratory as we can see in table 6.9.

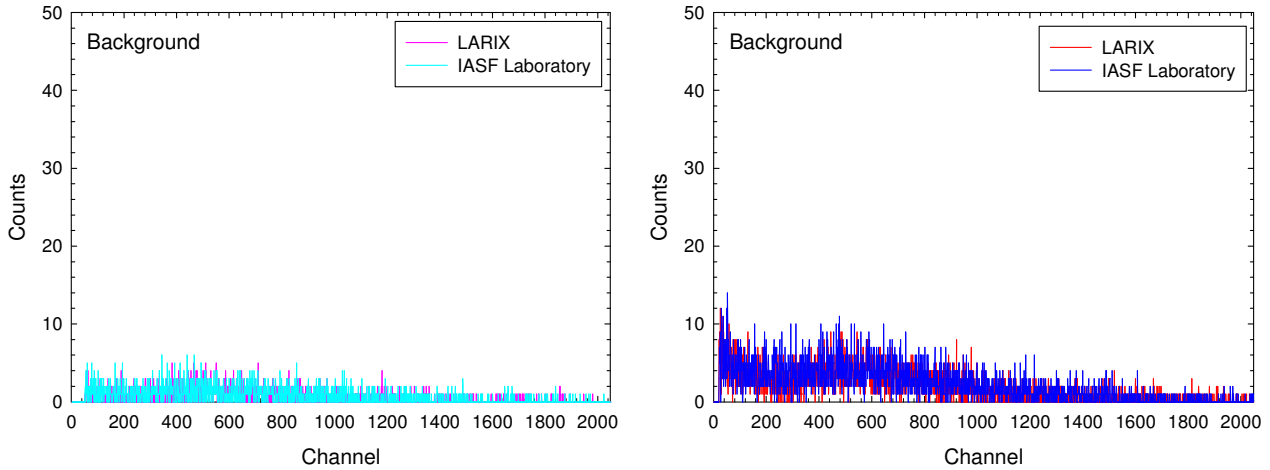


Figure 6.29. Comparison between the background inside the X-ray facility tunnel and one at IASF Bologna laboratory acquired in 100 (left) and 300 s (right).

Table 6.9. Background level at facility tunnel and at IASF Bologna laboratory.

	Background level 100 s	Background level 300 s
IASF Bologna Laboratory	1461	4376
LARIX	1183	3758



7. Test under X-Ray beam at LARIX

The focal plane detectors have been tested by illuminating them with the X-Ray beam supplied by Bosello High Technology at 200 kV and 0.2 mA at LARIX in the position in which a bent Ge crystal diffracts the photon beam. The X ray source was set to fine focus ($0.4 \times 0.6 \text{ mm}^2$) with the first W collimator hole of 3 mm in diameter.

In Figure 7.1 a zoomed region the image acquired in transmission with a Ge tile placed in the nominal Laue lens petal support position at the nominal Bragg angle is shown. In the image (2 s integration) it is clearly visible the radiography of the indented Ge tile. Due to the focal plane distance we expect an amplification of a factor 1.8 between the real collimator slit sizes and the spot recorded by the imager. This is confirmed by the measure in pixel of the rectangular spot shown in Figure 7.1(a): $\sim 36 \times 55$ pixels ($0.2 \times 0.2 \text{ mm}^2$ per pixel). The difference in gray levels between thick (2 mm) Ge region and thin (0.5 mm) ones is ~ 15 gray levels. The gray levels and therefore the corresponding signal in the thin Ge region are at about 2.2 sigma over the background rms values (6.7 gray levels), as shown in Figure 7.1 (b).

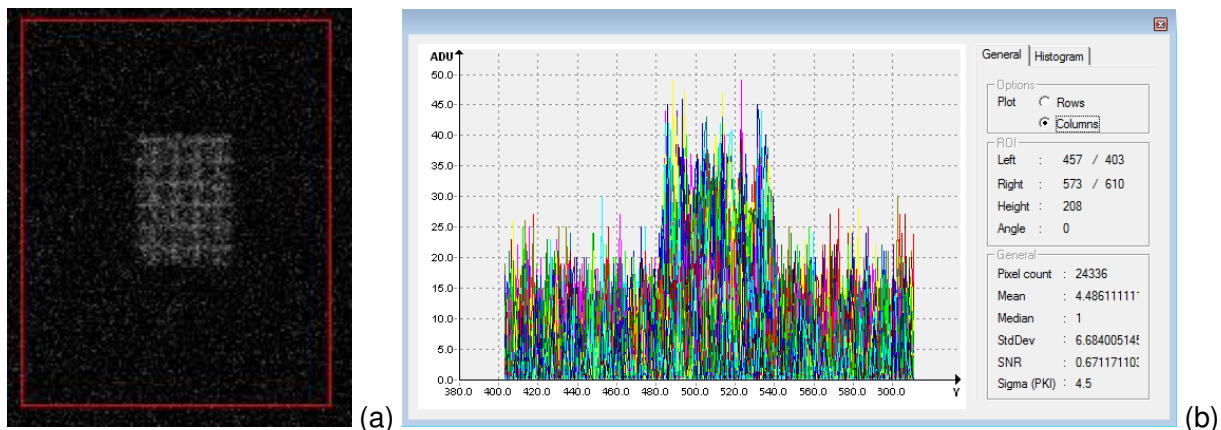


Figure 7.1. (a) The gray level image of the transmitted beam through a indented Ge tile at 200 kV and 0.2 mA; (b) the gray levels profile of a in the Y (horizontal/column) direction.

In Figure 7.2 the spectrum of transmitted beam at 200 kV and 0.2 mA is recorded with the HPGe detector setting a live acquisition time of 1000 s. All the high energy fluorescence lines ($k\alpha_1$ e $k\alpha_2$ lines at 59.3 and 57.9 keV, and $k\beta_1$ e $k\beta_2$ lines at 67.2 and 69 keV) emitted by the W target in the X ray source are well separated. The spectrum is obtained with a Ge tile placed in the nominal position on the Laue lens petal support at the nominal Bragg angle and the final W collimator slit was set at $4 \times 6 \text{ mm}^2$. In the insert of Figure 7.2, a zoomed region around 100 keV is shown to demonstrate the presence of a region with lack of counts due to the Bragg diffraction at this energy by the Ge crystal. From the spectrum it is possible to perform a first order evaluation of the crystal diffraction efficiency, that is $\sim 10\%$ (over 8 channel, i.e. $\sim 1.4 \text{ keV}$ energy band). This value is a lower limit because it does not take into account the convolution between the diffraction energy band (0.4 keV) and the finite detector energy resolution ($\sim 0.8 \text{ keV}$ FWHM at 100 keV).

All the results of tests performed and still undergoing at the X ray beam facility with the two focal plane detectors will be reported in a more detailed document that will be issued in the next couple of months.

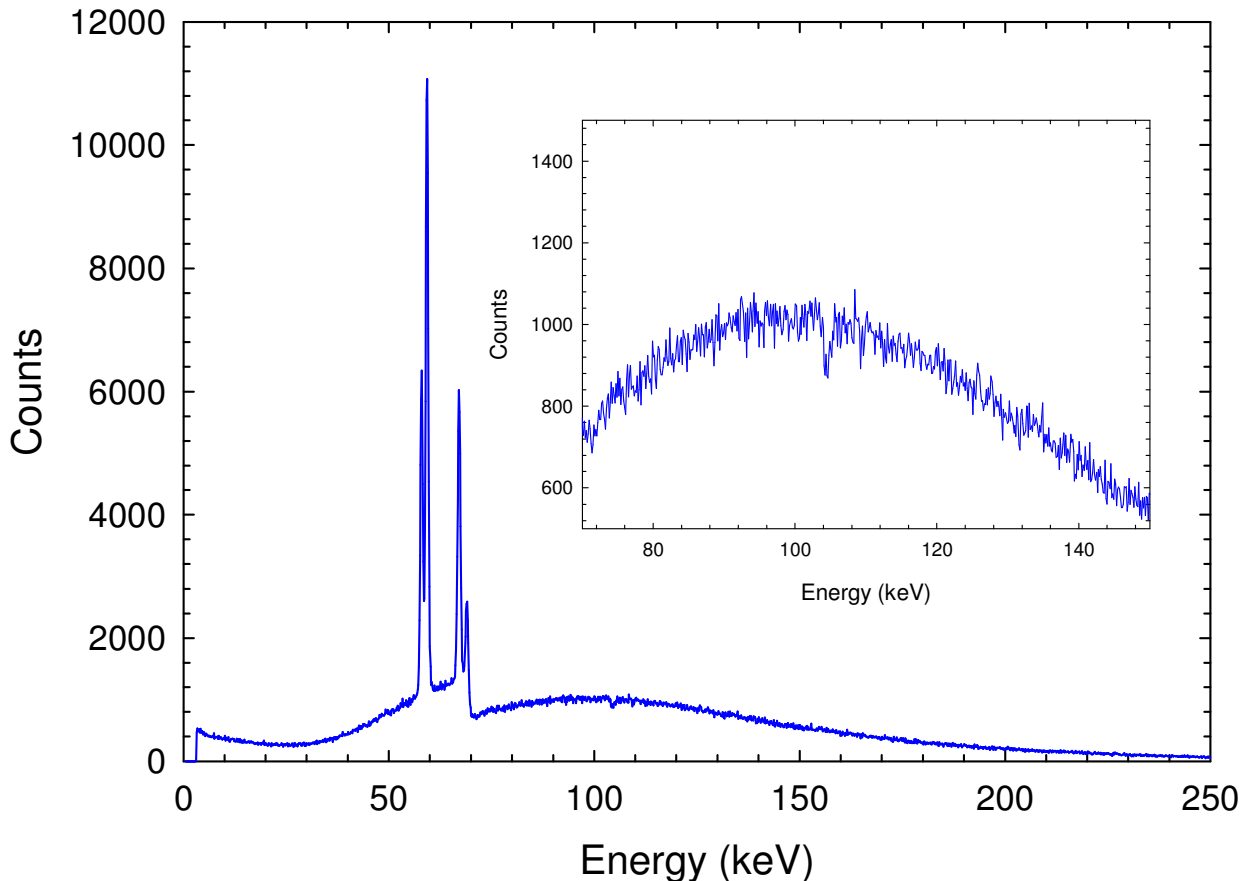


Figure 7.2. HPGe spectrum of the transmitted beam at 200 kV and 0.2 mA. The insert shows a zoomed region around 100 keV where the lack of counts in correspondence of the diffracted beam is clearly visible.

8. Images at a different focal length

Due to the LARIX facility experimental setup, in which the X ray beam is not parallel but from the X-ray tube, the beam divergence affects the bent crystal focusing effect, having as a consequence that the focal distance at which the bent crystals concentrate is minor than 20 m. To confirm this hypothesis, we have acquired some images with the focal plane flat panel at a focal length of 15 m by using a GaAs (#4.9) and a Ge (#68) crystal.

In Figure 8.1 we report the image obtained by irradiating the GaAs crystal with a collimator window of size 5 mm x 5 mm, in the position 33 at a nominal diffracted energy of about 150 keV and measured of 156.35 keV. The acquisition time is 510 s equivalent to 30 frames, each of 17 s in the external trigger mode. The settings of X-ray tube are:

- **voltage** = 250 keV
- **current** = 3 mA.

By using the same settings for the X Ray tube the focal spot at 15 m, recorded by irradiating the Ge crystal with a collimator window of size 15 mm x 5 mm, is shown in Figure 8.2. The diffracted energy



in this case is ~ 97 keV. The acquisition time in the external trigger mode of the image on the left is 510 s, while it is 170 s for one on the right equivalent at 10 frames, each of 17 s. The difference between the two images consists in the way of blocking of the crystal, which is mounted on the hexapod on the left and left free on the right. We can clearly note that in the first case the crystal focusing capability is lost, concluding that it is advisable to change the blocking mechanical device.

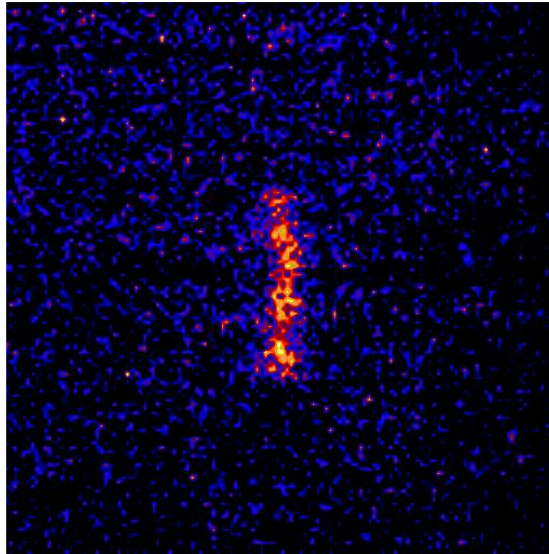


Figure 8.1. Diffracted beam spot at a focal distance of 15m by a GaAs crystal (128x128 pixels).

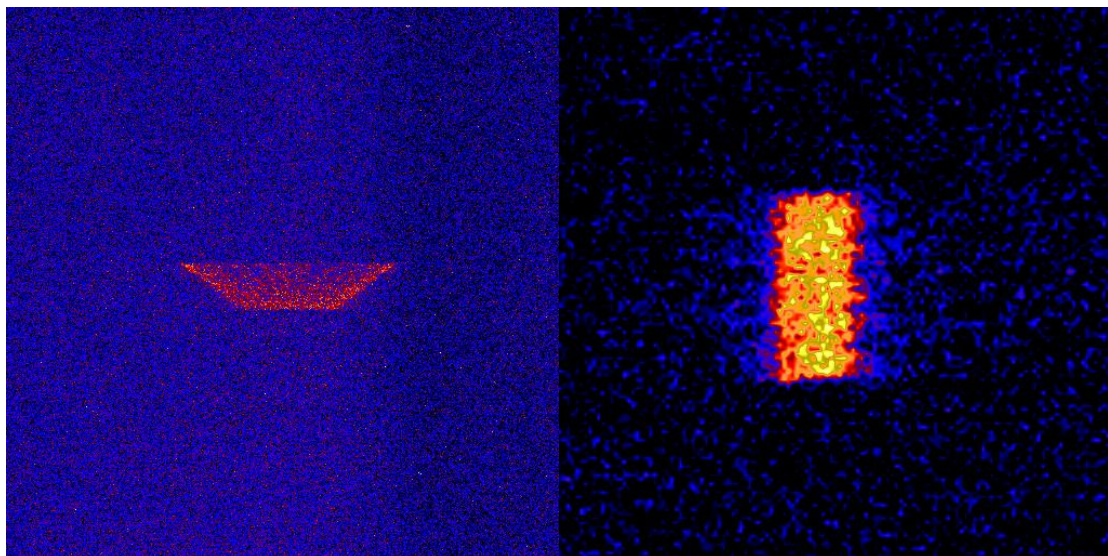


Figure 8.2. Diffracted beam spot at a focal distance of 15 m by a Ge crystal mounted on the hexapod (512x512 pixels) on the left and left free (128x128 pixels) on the right.

9. Beam intensity as a function of the collimator window

In the following figure the beam intensity is reported as a function of the size increasing of the collimator window. We can conclude that it is quite linear.

We have reported both the total counts summed in the selected ROI around the peak (Gross Area) and the total counts at which we have subtracted the background counts (Net Area). In the figure below the corresponding spectra are shown, acquired with the GaAs crystal at a diffracted energy of 156.35 keV.

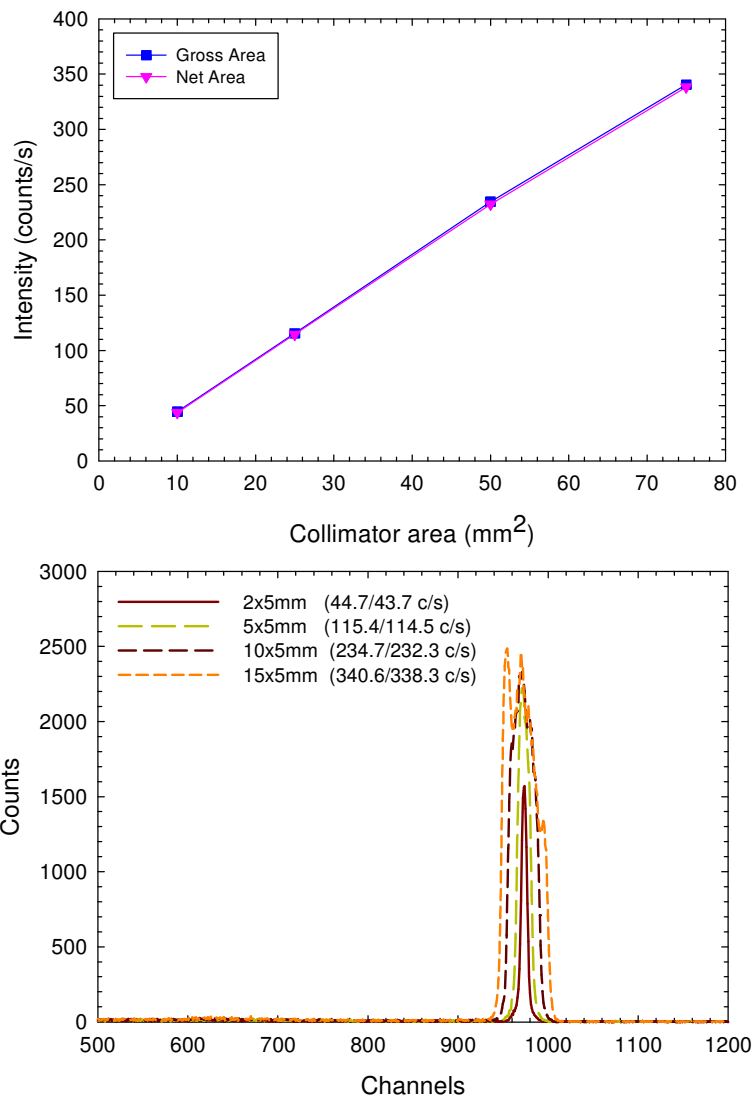


Figure 9.1. Beam intensity vs collimator window size (above): relative spectra (below).

10. Conclusions

In this report we have analysed and verified the functionality of the EGSE detectors, including the sensors, the electronics and the acquisition software. We have illustrated the characterization and the calibration of the two focal plane detectors performed before and after integrating in the X-ray beam line at the LARIX facility in Ferrara.

We can confirm that our choice concerning the kind of focal plane detectors was appropriate, because the project requirements are well fulfilled.